NTNU
Norwegian University of
Science and Technology

A molecular dynamics study of prolate ellipsoidal nanoparticles adsorbed at liquid-vapour interfaces

Olav Galteland

Chemistry	
Submission date:	May 2017
Supervisor:	Bjørn Hafskjold, IKJ
Co-supervisor:	Fernando Bresme, IKJ

Norwegian University of Science and Technology
Department of Chemistry

Abstract

Nanoparticles may adsorb strongly at liquid-vapour interfaces and form layers, which may be a source for new and interesting materials. It is not fully understood how the nanoparticles adsorbed at the interface interact, and how the shape and size of the nanoparticles affect the interaction. Prolate ellipsoidal nanoparticles will deform the interface, which leads to strong orientation-dependent capillary interactions. This will result in nanoparticle self-assembly.

A molecular dynamics method for modelling prolate ellipsoidal nanoparticles interacting with spherical fluid particles is described. The method was used to calculate the wetting, Brownian motion and interface deformation of nanoparticles adsorbed at liquid-vapour interfaces. The force between two nanoparticles adsorbed at an interface and two nanoparticles submerged in bulk phases was also calculated. Nanoparticle sizes ranging from approximately 0.3 nm to 5.0 nm were considered. Two different potentials have been considered for the prolate ellipsoidal nanoparticles, one with the same interaction energy all around the nanoparticle and one with higher interaction energy on the sides of the nanoparticle compared to the tip.

Highly wetting prolate ellipsoidal nanoparticles with a higher interaction energy on the sides compared to the tips were found to prefer an equilibrium orientation where the long axis of the nanoparticle is normal to the interface. The Brownian motion of prolate ellipsoidal nanoparticles suggests that they diffuse primarily along the long axis of the nanoparticle. Interface deformation of prolate ellipsoidal nanoparticles of this size was not observed. The force between nanoparticles was calculated, and used to predict the behaviour of nanoparticles adsorbed at liquid-vapour interfaces. Orientation-dependent capillary interaction between prolate ellipsoidal nanoparticles was not observed.

Sammendrag

Nanopartikler kan adsorbere sterkt på gass-væske grenseflater og danne lag av nanopartikler, som kan være en kilde til nye og interessante materialer. Det er ikke fullstendig forstått hvordan formen og størrelsen på nanopartiklene påvirker interaksjonen. Prolate ellipsoidale nanopartikler vil deformere grenseflaten, noe som fører til sterke orienteringsavhengige kapillærkrefter. Dette fører til selvorganisering av nanopartikler.

En molekyldynamikk-metode for modellering av prolate ellipsoidale nanopartikler med sfæriske fluidpartikler blir presentert. Metoden har blitt brukt til å beregne fukting, selvdiffusjon, og deformasjon av grenseflaten. Kraften mellom to nanopartikler adsorbert på grenseflaten og to nanopartikler nedsenket i bulkfasen har også blitt beregnet. Nanopartikler med størrelser mellom omtrent 0.3 nm til 5.0 nm har blitt undersøkt. To ulike potensialer har blitt undersøkt for de prolate ellipsoidale nanopartiklene, én med lik interaksjonsenergi rundt hele nanopartikkelen og én med sterkere interaksjonsenergi på sidene av nanopartikkelen i forhold til tuppen.

Det har blitt oppdaget at høyt fuktende prolate ellipsoidale nanopartikler med høy interaksjonsenergi på sidene i forhold til tuppen, vil foretrekke en likevektsorientering hvor nanopartikkelens lange akse er normal til grenseflaten. Selvdiffusjonen av prolate ellipsoidale nanopartikler tyder på at de hovedsaklig diffunderer langs nanopartikkelens lange akse. Grenseflatedeformasjonen på grunn av prolate ellipsoidale nanopartiklene av denne størrelsen har ikke blitt observert. Kreftene mellom nanopartikler har blitt beregnet, og blitt brukt til å forutsi oppførselen til nanopartikler som er adsorbert på grenseflaten.

Acknowledgements

I would like to thank to my supervisor professor Bjørn Hafskjold, who has been the best supervisor anyone could ask for.

Thanks to my co-supervisor professor Fernando Bresme for hosting me at Imperial College London, and for many meaningful discussions.

Thanks to Juan David Olarte Plata at Imperial College London for helping me with molecular dynamics simulations, and for many meaningful discussions.

Thanks to the KIFEE-9 leadership for organising a great symposium, and for hosting me during my stay in Kyoto.

Thanks to Lilja Brekke Thorfinnsdottir and Peder Notto Galteland for proofreading of this thesis.

Computer resources have been provided by Faculty of Natural Science at NTNU, the HPC resources at UiT and NTNU provided by NOTUR (www.sigma2.no), and the Imperial College High Performance Computing Service.

Contents

1 Introduction **19**

1.1 Motivation 19

1.2 Outline 21

2 Theory **23**

2.1 Thermodynamic models 23

2.2 Nanoparticles at fluid interfaces 25

2.2.1 Wetting 25

2.2.2 Brownian motion 27

2.2.3 Interface deformation 28

2.3 Forces acting on nanoparticles at fluid interfaces 29

2.3.1 Van der Waals force 29

2.3.2 Solvent-mediated forces 30

2.3.3 Capillary forces 30

3 Methodology **33**

3.1 Molecular dynamics simulation 33

3.1.1 Non-spherical particles 34

3.1.2 Force fields 35

3.1.3 Reduced units 37

3.1.4 Thermostat 37

3.1.5 Periodic boundaries 38

3.2 Simulation details 38

3.2.1 Force fields 39

3.2.2 Comparison with a Lennard-Jones crystals 42

3.2.3 Two-phase system 42
3.2.4 Wetting 43
3.2.5 Brownian motion 43
3.2.6 Interface deformation 43
3.2.7 Solvent-mediated forces 44
3.3 Estimating errors 44

4 Results and discussion 47
4.1 Comparison with a Lennard-Jones crystal 47
4.2 Two-phase system 48
4.3 Wetting properties 49
4.3.1 Pitch 51
4.4 Brownian motion 56
4.5 Interface deformation 61
4.6 Solvent-mediated forces 63
4.6.1 Spherical nanoparticles 64
4.6.2 Prolate ellipsoidal nanoparticles 67
4.6.3 Summary of solvent-mediated forces 71

5 Conclusion 73

Appendices 75

A Force fields 75

B LAMMPS input scripts 79

List of Figures

2.1 **(a)** Spherical nanoparticle of radius R adsorbed at a liquid-vapour interface. l is a vector distance from the interface to the nanoparticle centre. **(b)** A prolate ellipsoidal nanoparticle of radii $a > b = c$ adsorbed to a liquid-vapour interface, where c is the radius of the prolate ellipsoidal nanoparticle normal to the ab-plane, and l is a vector distance from the interface to the nanoparticle centre. 24

2.2 Side view of a prolate ellipsoidal nanoparticle adsorbed at a liquid-vapour interface inducing interface deformations. **(a)** A prolate ellipsoidal nanoparticle laying flat on the interface. Δh is the maximal meniscus height of the deformation and l is the distance from the nanoparticle centre to the interface position. **(b)** A prolate ellipsoidal nanoparticle that is tilted with pitch ϕ. 29

2.3 **(a)** Top-down view of two prolate ellipsoidal nanoparticles adsorbed at a liquid-vapour interface. a and b are the radii of the nanoparticle, and d is the surface-to-surface distance. **(b)** Top-down view of two prolate ellipsoidal nanoparticles adsorbed to a liquid-vapour interface. The vectors $\boldsymbol{e}_i$ and $\boldsymbol{e}_j$ indicate the orientation of nanoparticle i and j respectively. α_{ij} is the angle between vector $\boldsymbol{e}_i$ and $\boldsymbol{e}_j$, and $\boldsymbol{r}_{ij}$ is the centre-to-centre nanoparticle separation. 30

2.4 Top-down view of possible prolate-prolate configurations, **(a)** side-by-side, **(b)** tip-to-side and **(c)** tip-to-tip. 31

3.1 The potential energy between a fluid particle and a nanoparticle of radii $a = 7.5\sigma_0, b = c = 2.5\sigma_0$ and well depth $\epsilon_{fp} = 3\epsilon_0$, and relative well depth ratios **(a, c)** $\kappa' = 5$ and **(b, d)** $\kappa' = 1$. The well depth ϵ_{fp} does not correspond to the real energy minimum. See text for details. 40

3.2 Potential energy of the fluid-nanoparticle interaction for a nanoparticle with well depth $\epsilon_{fp} = 3\epsilon_0$ and of radii **(a)** $a = 5\sigma_0, b = c = 2.5\sigma_0$, and **(b)** $a = 7.5\sigma_0, b = c = 2.5\sigma_0$. 41

4.1 **(a)** Snapshot of a fluid particle in red and a prolate ellipsoidal face-centred cubic crystal in blue. A prolate ellipsoid was superimposed over the crystal. **(b)** The potential energy of a fluid particle as a function of the distance between a fluid particle and the tip and side of a prolate ellipsoid face-centred cubic crystal consisting of Lennard-Jones particles. 47

4.2 **(a)** Snapshot of the simulation box after equilibration. The fluid particles are shown in red. **(b)** Density profile of the two-phase system after equilibration along the x-axis. 49

4.3 **(a)** A top-down snapshot of a nanoparticle of radii $a = 7.5\sigma_0, b = c = 2.5\sigma_0$ adsorbed at a liquid-vapour interface. **(b)** The wetting of a nanoparticle of size $a = 7.5\sigma_0, b = c = 2.5\sigma_0$ during equilibration. **(c)** The density profile of the liquid-vapour interface, and three nanoparticles of radii $a = 7.5\sigma_0, b = c = 2.5\sigma_0$ with wettabilities $\frac{l}{b} = 0$ (red), $\frac{l}{b} = -1$ (blue), and $\frac{l}{b} = 1$ (green). The dotted line represents Gibbs dividing surface. 50

4.4 Nanoparticles of well depth ratio $\kappa' = 5$. The mean wetting $\langle \frac{l}{b} \rangle$ of nanoparticles of radii $a = 7.5\sigma_0, b = c = 2.5\sigma_0$, $a = 5.0\sigma_0, b = c = 2.5\sigma_0$, $a = 4.5\sigma_0, b = c = 1.5\sigma_0$ and $a = 1.5\sigma_0, b = c = 0.5\sigma_0$ as a function of well depth ϵ_{fp}. 51

4.5 Nanoparticles of well depth ratio $\kappa' = 1$. The mean wetting $\langle \frac{l}{b} \rangle$ of nanoparticles of radii $a = 7.5\sigma_0, b = c = 2.5\sigma_0$, $a = 5.0\sigma_0, b = c = 2.5\sigma_0$, $a = b = c = 2.5\sigma_0$, $a = 4.5\sigma_0, b = c = 1.5\sigma_0$ and $a = 1.5\sigma_0, b = c = 0.5\sigma_0$ as a function of well depth ϵ_{fp}. 52

4.6 The mean pitch, $\langle \phi \rangle$, as a function of wetting, $\frac{l}{b}$, for a nanoparticle of size $a = 7.5\sigma_0, b = c = 2.5\sigma_0$. Nanoparticles with well depth ratio **(a)** $\kappa' = 5$ and **(b)** $\kappa' = 1$. 53

4.7 The mean pitch, $\langle \phi \rangle$, as a function of wetting, $\frac{l}{b}$, for a nanoparticle of size $a = 5.0\sigma_0, b = c = 2.5\sigma_0$. Nanoparticles with well depth ratio **(a)** $\kappa' = 5$ and **(b)** $\kappa' = 1$. 54

4.8 The mean pitch, $\langle\phi\rangle$, as a function of wetting, $\frac{l}{b}$, for a nanoparticle of size $a = 4.5\sigma_0, b = c = 1.5\sigma_0$. Nanoparticles with well depth ratio **(a)** $\kappa' = 5$ and **(b)** $\kappa' = 1$. 55

4.9 The mean pitch, $\langle\phi\rangle$, as a function of wetting, $\frac{l}{b}$, for a nanoparticle of size $a = 1.5\sigma_0, b = c = 0.5\sigma_0$. Nanoparticles with well depth ratio **(a)** $\kappa' = 5$ and **(b)** $\kappa' = 1$. 55

4.10 The Brownian motion of **(a)** a prolate ellipsoidal nanoparticle of radii $a = 7.5\sigma_0, b = c = 2.5\sigma_0$ and wetting $\langle\frac{l}{b}\rangle = -0.02 \pm 1.50 \times 10^{-3}$, and **(b)** a spherical nanoparticle of radii $a = b = c = 2.5\sigma_0$ and wetting $\langle\frac{l}{b}\rangle = -0.05 \pm 2.17 \times 10^{-3}$. 57

4.11 The Brownian motion of **(a)** a prolate ellipsoidal nanoparticle of radii $a = 7.5\sigma_0, b = c = 2.5\sigma_0$ and wetting $\langle\frac{l}{b}\rangle = -0.98 \pm 2.26 \times 10^{-3}$, and **(b)** a prolate ellipsoidal nanoparticle of radii $a = 7.5\sigma_0, b = c = 2.5\sigma_0$ and wetting $\langle\frac{l}{b}\rangle = 1.04 \pm 3.19 \times 10^{-3}$. 58

4.12 Mean-square displacement of nanoparticles adsorbed at the liquid-vapour interface. **(a)** Nanoparticles of radii $a = 7.5\sigma_0, b = c = 2.5\sigma_0$ and wettabilities $\langle\frac{l}{b}\rangle = -0.98 \pm 2.26 \times 10^{-3}$ in red, $\langle\frac{l}{b}\rangle = 0.02 \pm 1.50 \times 10^{-3}$ in blue, and $\langle\frac{l}{b}\rangle = 1.04 \pm 3.19 \times 10^{-3}$ in green. **(b)** Nanoparticles of radii $a = 7.5\sigma_0, b = c = 2.5\sigma_0$ and $a = b = c = 2.5\sigma_0$ with wettabilities $\langle\frac{l}{b}\rangle = 0.02 \pm 1.50 \times 10^{-3}$ and $\langle\frac{l}{b}\rangle = 0.05 \pm 2.17 \times 10^{-3}$, respectively. 59

4.13 The two-dimensional self-diffusion coefficient, D, as a function of wetting, $\frac{l}{b}$, for nanoparticles of radii $a = 7.5\sigma_0, b = c = 2.5\sigma_0$ (red circle) and $a = b = c = 2.5\sigma_0$ (blue square). 60

4.14 Local density of fluid particles in a slab of thickness equal to the short diameter of the nanoparticle, $2b = 5.0\sigma_0$, around the nanoparticle adsorbed at a liquid-vapour interface. The nanoparticles are of well depth ratio $\kappa' = 5$ and **(a)** radii $a = 7.5\sigma_0, b = c = 2.5\sigma_0$ and wetting $l/b = 0.628$, and **(b)** radii $a = 5.0\sigma_0, b = c = 2.5\sigma_0$ and wetting $l/b = 0.676$. 61

4.15 Snapshot of nanoparticles of well depth ratio $\kappa' = 5$ and radii **(a)** $a = 7.5\sigma_0, b = c = 2.5\sigma_0$ and **(b)** $a = 5.0\sigma_0, b = c = 2.5\sigma_0$ adsorbed at a liquid-vapour interface. The fluid particles in red are in a slab around the nanoparticles in blue. 62

4.16 Local density of fluid particles in a slab of thickness equal to the short diameter of the nanoparticle, $2b = 5.0\sigma_0$, around the nanoparticle adsorbed at a liquid-vapour interface. The nanoparticles are of well depth ratio $\kappa' = 1$ and **(a)** radii $a = 7.5\sigma_0, b = c = 2.5\sigma_0$ and wetting $l/b = 0.710$, and **(b)** radii $a = 5.0\sigma_0, b = c = 2.5\sigma_0$ and wetting $l/b = 0.692$. 63

4.17 **(a)** A top-down snapshot of a nanoparticle-nanoparticle pair of size $a = 7.5\sigma_0, b = c = 2.5\sigma_0$, surface-to-surface separation $d = 0\sigma_0$, and well depth ratio $\kappa' = 1$ adsorbed at a liquid-vapour interface. **(b)** Solvent-mediated force acting on a spherical nanoparticle of radii $a = b = c = 2.5\sigma_0$ and well depth ratio $\kappa' = 1$ as a function of surface-to-surface separation d. 64

4.18 **(a)** Solvent-mediated force acting on a spherical nanoparticle of radii $a = b = c = 2.5\sigma_0$ and well depth ratio $\kappa' = 1$ as a function of surface-to-surface separation d. The nanoparticles are submerged in bulk liquid. **(b)** Two spherical nanoparticles (red) with a separation $d < 1\sigma_0$. Fluid particles (blue) are acting on the nanoparticles. If the spherical nanoparticles have a large well depth ϵ_{fp}, the fluid particles will want to stay between the two nanoparticles. 65

4.19 **(a)** Solvent-mediated force acting on a prolate ellipsoidal nanoparticle of radii $a = 7.5\sigma_0, b = c = 2.5\sigma_0$ and well depth ratio $\kappa' = 1$ as a function of surface-to-surface separation d in the side-by-side orientation. **(b)** Two prolate ellipsoidal nanoparticles (red) with a separation $d < 1\sigma_0$. Fluid particles (blue) are packing on the tips and creating oscillations in the depletion region. 67

4.20 Solvent-mediated force acting on a prolate ellipsoidal nanoparticle with well depth ratio $\kappa' = 1$ as a function of surface-to-surface separation d. The nanoparticles are of radii $a = 7.5\sigma_0, b = c = 2.5\sigma_0$ in the side-by-side (SS), side-to-tip (ST) and tip-to-tip (TT) orientations. 68

4.21 **(a)** Nanoparticles of radii $a = 7.5\sigma_0, b = c = 2.5\sigma_0$ in the side-to-tip orientation. This shows that the force on both particles is the same even when the orientation is non-symmetric. **(b)** Two prolate ellipsoidal nanoparticles (red) in the side-to-tip orientation and fluid particles (blue). The fluid particles are pushing on the particle 1 in such a way that the total force on particle 1 equals the total force acting on particle 2. 69

4.22 Solvent-mediated force acting on a prolate ellipsoidal nanoparticle with well depth ratio $\kappa' = 1$ as a function of surface-to-surface separation d. **(a)** Nanoparticles of radii $a = 7.5\sigma_0, b = c = 2.5\sigma_0$ in the side-by-side orientation, with wettabilities $\frac{l}{b} = 0.51 \pm 9.32 \times 10^{-5}$, $\frac{l}{b} = -0.08 \pm 2.94 \times 10^{-4}$ and $\frac{l}{b} = -0.70 \pm 4.22 \times 10^{-5}$. **(b)** Nanoparticles of radii $a = 7.5\sigma_0, b = c = 2.5\sigma_0$, $a = 5.0\sigma_0, b = c = 2.5\sigma_0$ and $a = 4.5\sigma_0, b = c = 1.5\sigma_0$ in the side-by-side orientation. 70

4.23 Solvent-mediated force acting on a prolate ellipsoidal nanoparticle of radii $a = 7.5\sigma_0, b = c = 2.5\sigma_0$, $a = 5.0\sigma_0, b = c = 2.5\sigma_0$ and $a = 4.5\sigma_0, b = c = 1.5\sigma_0$ with well depth ratio $\kappa' = 1$ as a function of surface-to-surface separation d. 71

A.1 Potential energy of the nanoparticle-fluid interaction with well depth ratio $\kappa' = 5$. r_{fp} is the cut-off. **(a)** Nanoparticle of size $a = 7.5\sigma_0, b = c = 2.5\sigma_0$ and well depth $\epsilon_{fp} = 3.0\epsilon_0$, **(b)** nanoparticle of size $a = 5.0\sigma_0, b = c = 2.5\sigma_0$ and well depth $\epsilon_{fp} = 3.0\epsilon_0$, **(c)** nanoparticle of size $a = 4.5\sigma_0, b = c = 2.5\sigma_0$ and well depth $\epsilon_{fp} = 2.0\epsilon_0$ and **(d)** nanoparticle of size $a = 1.5\sigma_0, b = c = 0.5\sigma_0$ and well depth $\epsilon_{fp} = 1.0\epsilon_0$. 76

A.2 Potential energy of the nanoparticle-fluid interaction with well depth ratio $\kappa' = 1$. r_{fp} is the cut-off. **(a)** Nanoparticle of size $a = 7.5\sigma_0, b = c = 2.5\sigma_0$ and well depth $\epsilon_{fp} = 3.0\epsilon_0$, **(b)** nanoparticle of size $a = 5.0\sigma_0, b = c = 2.5\sigma_0$ and well depth $\epsilon_{fp} = 3.0\epsilon_0$, **(c)** nanoparticle of size $a = 4.5\sigma_0, b = c = 2.5\sigma_0$ and well depth $\epsilon_{fp} = 2.0\epsilon_0$ and **(d)** nanoparticle of size $a = 1.5\sigma_0, b = c = 0.5\sigma_0$ and well depth $\epsilon_{fp} = 1.0\epsilon_0$. 77

A.3 Potential energy of the nanoparticle-fluid interaction with well depth ratio $\kappa' = 1$ and nanoparticle radii $a = b = c = 2.5\sigma_0$ and well depth $\epsilon_{fp} = 3.0$. . 78

List of Tables

3.1 Definition of Lennard-Jones reduced units 38

A.1 Gay-Berne parameters for fluid-nanoparticle interaction. 75

List of symbols

Symbol	Description
F	Helmholtz free energy
T	Temperature
V	Volume
N	Number of particles
A	Interface area
L	Length of the three-phase line
γ	Interface tension
τ	Line tension
θ	Contact angle
a	Long radius of prolate nanoparticle.
b	Short radius of prolate nanoparticle.
c	Short radius of prolate nanoparticle.
R	Radius of spherical nanoparticles.
l	Distance from nanoparticle centre to interface position.
d	Nanoparticle-nanoparticle surface-to-surface separation.
κ	Particle aspect ratio.
Δh	Meniscus height of interface deformation.
$\mathbf{e_i}$	Orientation of prolate ellipsoidal nanoparticle i.
$\mathbf{r_{ij}}$	Distance from centre of nanoparticle i to centre of nanoparticle j.
α_{ij}	Angle between prolate nanoparticle i and j.
u_{ij}	Potential energy of particle i due to particle j.
ρ	Density
$\boldsymbol{f}_i$	Force acting on particle i.
t	Time

$\boldsymbol{v}_i$	Velocity of particle i.
$\mathbb{A}_i$	Rotation matrix of particle i.
$\boldsymbol{Q}_i$	Quaternions of particle i
q_i	Quaternion i.
$\boldsymbol{\tau}_i$	Torque of particle i.
$\boldsymbol{I}_i$	Moment of inertia of particle i.
$\boldsymbol{\omega}_i$	Angular velocity of particle i.
σ_{ij}	Lennard-Jones parameter that determines particle size.
ϵ_{ij}	Lennard-Jones parameter that determined interaction strength.
κ'	Well depth ratio of a prolate ellipsoidal nanoparticle

Conventions

- Variables with a superscript asterisk are in Lennard-Jones units, *e.g.* x^*.
- Variables in normal typeface are scalars, *e.g.* x.
- Variables in bold typeface are vectors, *e.g.* $\mathbf{x}$.
- Variables in blackboard bold are matrices, *e.g.* $\mathbb{X}$.
- The Euclidean norm is denoted with double vertical lines, *e.g.* $\|x\|$.
- The dot product is denoted with a dot, *e.g.* $\mathbf{x} \cdot \mathbf{y}$.
- The cross product is denoted with a cross, *e.g.* $\mathbf{x} \times \mathbf{y}$.
- Variables with one subscript specify a quantity related to a single particle, *e.g.* x_i.
- Variables with two subscripts specify a quantity related to a particle pair, *e.g.* x_{ij}.

Chapter 1

Introduction

1.1 Motivation

The study of nanoparticles and their interaction with interfaces is important in the understanding and application of a wide range of problems. A nanoparticle is a solid of size ranging from 1 nm to 100 nm, and an interface is the border between two phases. Nanoparticle and interface science are important in the chemical industry, as a report from the chemical company DuPont notes [1]. They reported that roughly 60% of their products are marketed as powders, dispersions, or suspensions.

Attraction between nanoparticles may result in aggregation or self-assembly [2]. Aggregation is the phenomenon where nanoparticles "clump together" creating clusters that are kinetically stable, while self-assembly is the phenomenon where they aggregate in an organised and predictable way. If the attraction is understood and controlled, it might be possible to create macroscopic solids with tailored properties. It has been shown in experiments by Rozynek *et al.* [3] and Dommersnes *et al.* [4] that it is possible to create interesting materials, such as Janus and patchy capsules. These materials may be used to encapsulate entities such as molecules, particles, or bubbles, while still having the property of Janus or patchy particles. They used an electromagnetic field to assemble particles in a ribbon shape on the surface of a sessile drop. Davies *et al.* [5] studied prolate ellipsoidal nanoparticles and how they assemble in interesting patterns on a fluid-fluid interface using continuum simulations. They showed the potential these nanoparticles has for creating new materials.

Research is needed to take advantage of this technology. Much research has been done on this topic in the last 20 years, but the effects of particle shape, surface curvature and particle characteristics are still not fully understood. How the particle shape affect the forces between nanoparticles adsorbed at liquid-vapour interfaces is important to understand in order to predict and exploit the aggregation or self-assembly of nanoparticles, which may be a source of new and interesting materials. Loudet *et al.* [6] observed prolate ellipsoidal mosquito eggs of size 1 mm floating at an air-water interface self-assemble. This is argued to be caused by strong long-ranged capillary interactions. Lehle *et al.* [7] concluded that prolate ellipsoidal nanoparticles adsorbed at liquid-vapour interfaces deform the interface, which leads to orientation-dependent capillary interactions. Dasgupta *et al.* [8] used continuum simulations to determine the magnitude of the capillary interaction, and they confirmed that the capillary interactions are of the order of $10^8 k_B T$ for micrometer-sized prolate ellipsoidal nanoparticles.

The aim of this thesis is to establish a molecular dynamics method to model prolate ellipsoidal nanoparticles adsorbed at liquid-vapour interfaces, perform calculations that predict their behaviour, and identify the capillary force caused by nanoparticle shape. Molecular dynamics simulations with the Lennard-Jones and Gay-Berne force fields were used. The Lennard-Jones force field model van der Waals forces for spherical fluid particles, and the Gay-Berne force field model van der Waals forces for prolate ellipsoidal nanoparticles. Molecular dynamics simulations are advantageous because it combines the microscopic and the macroscopic view of a system. The fluid particles are modelled individually as spherical particles, and not as a continuum. This results in the force changing dramatically when the size of the nanoparticle approaches the fluid particle size. Nanoparticle sizes ranging from approximately 0.3 nm to 5.0 nm were studied. Four aspects of the nanoparticles have been considered:

1. Wetting of nanoparticles, *i.e.* how the nanoparticle orients and positions itself in relation to the liquid-vapour interface.

2. Brownian motion of the nanoparticles adsorbed at a liquid-vapour.

3. Interface deformations as a result of the shape of prolate ellipsoidal nanoparticles.

4. The force between the nanoparticles adsorbed at liquid-vapour interfaces and in bulk liquid and vapour.

1.2 Outline

This thesis consists of three main parts: Theory, methodology, and results and discussion. The theory chapter presents relevant theory of prolate ellipsoidal nanoparticles adsorbed at liquid-vapour interfaces. The methodology chapter discusses the methods used to model nanoparticles adsorbed at liquid-vapour interfaces. The results and discussion chapter presents the results found in this work, and discusses their significance.

Chapter 2

Theory

This chapter presents theory relevant to prolate ellipsoidal nanoparticles adsorbed at liquid-vapour interfaces.

2.1 Thermodynamic models

The Helmholtz free energy of a nanoparticle adsorbed to a liquid-vapour interface may be described as,

$$F = F(T, V, N_1, N_2, A_{lv}, A_{sl}, A_{sv}, L), \tag{2.1}$$

where T is the temperature, V is the volume, N_i is the number of nanoparticles of species i, A_{lv} is the interface area of the liquid-vapour interface, A_{sv} is the interface area of the nanoparticle-vapour interface, A_{sl} is the interface area of the nanoparticle-liquid interface and L is the length of the three phase line [9]. The three phase line is the line where all three phases meet. The interface and line tension are defined as

$$\gamma_{ij} = \left(\frac{\partial F}{\partial A_{ij}}\right)_{T,V,N_1,N_2,A_{kl\neq ij},L}, \qquad \tau = \left(\frac{\partial F}{\partial L}\right)_{T,V,N_1,N_2,A_{ij}}. \tag{2.2}$$

The magnitude of the interface tension is of the order $10^{-3}\,\mathrm{N\,m^{-1}}$. The line tension is minuscule for large nanoparticles, but is thought to be of the order $10^{-8}\,\mathrm{N}$ to $10^{-12}\,\mathrm{N}$ for small nanoparticles [9]. The free energy associated with moving the nanoparticle immersed in one phase to the interface may be written as

$$\Delta F_{\text{int}} = F - F_0 = (\gamma_{sl} - \gamma_{sv})A_{sl} - \gamma_{lv}A_{st} + \tau L, \tag{2.3}$$

where A_{st} is the interface area between the two phases that is removed as a result of the nanoparticle, and F_0 is the free energy of the nanoparticle fully immersed in the

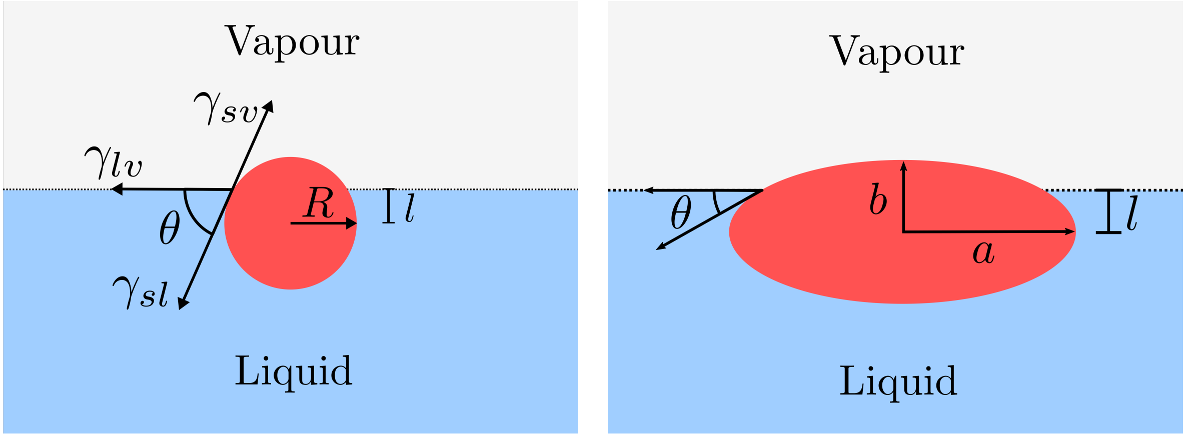

(a) **(b)**

Figure 2.1: **(a)** Spherical nanoparticle of radius R adsorbed at a liquid-vapour interface. l is a vector distance from the interface to the nanoparticle centre. **(b)** A prolate ellipsoidal nanoparticle of radii $a > b = c$ adsorbed to a liquid-vapour interface, where c is the radius of the prolate ellipsoidal nanoparticle normal to the ab-plane, and l is a vector distance from the interface to the nanoparticle centre.

vapour phase. Aveyard and Clint [10] derived the free energy for the case of spherical nanoparticles,

$$\Delta F_{\text{int}}^{\text{sphere}} = A_p \gamma_{lv} \left(-\frac{1}{4}(1-\bar{l}) + \frac{1}{2}\cos\theta(1-\bar{l}) + \frac{1}{2}\bar{\tau}\sqrt{1-\bar{l}^2} \right) \tag{2.4}$$

where θ is the contact angle, and $\bar{\tau}$ and $\bar{l}$ are defined as,

$$\bar{\tau} = \frac{\tau}{\gamma_{lv}}\sqrt{\frac{4\pi}{A_p}}, \qquad \bar{l} = \frac{l}{R}. \tag{2.5}$$

A_p is the surface area of the nanoparticle, l is the immersion depth and R is the nanoparticle radius, as depicted in figure 2.1a. The immersion depth is the distance from the nanoparticle centre to the interface position. The contact angle θ is the angle between the tangent line at the nanoparticle-interface intersection and the interface, as shown in figure 2.1a. By convention the contact angle is measured on the liquid side. According the modified Young-Dupré's equation, the relation between the contact angle and the interface tensions at a liquid-vapour interface for a stable configuration is

$$\cos\theta = \frac{\gamma_{sv} - \gamma_{sl}}{\gamma_{lv}} \left(1 - \frac{\tau}{R\gamma_{lv}\sin\theta} \right)^{-1}. \tag{2.6}$$

If the effect of the line tension is assumed to be infinitesimal, this reduces the Young-Dupré's equation to Young's equation,

$$\cos\theta = \frac{\gamma_{sv} - \gamma_{sl}}{\gamma_{lv}}. \tag{2.7}$$

This relation may be derived by considering a force balance of a spherical nanoparticle adsorbed to an interface, as seen in figure 2.1a. The components parallel to γ_{sl} and γ_{sv} must equal zero. A geometrical consideration confirms that $\gamma_{sl} + \gamma_{lv}\cos\theta = \gamma_{sv}$, which is Young's equation.

The immersion depth is defined such that $l = 0$ when $\theta = \frac{\pi}{2}$. Faraudo and Bresme [11] extended the free energy to the case of prolate ellipsoidal nanoparticles,

$$\Delta F_{\text{int}}^{\text{prolate}} = 4\pi R^2 \gamma_{lv} \left(-\frac{1}{4G(\kappa)}(1-\bar{l}^2) + \cos\theta A_{sl}\bar{l} + \bar{\tau}\frac{1}{2\sqrt{G(\kappa)}}\sqrt{1-\bar{l}^2} \right), \tag{2.8}$$

where κ is the aspect ratio of the nanoparticle defined $\kappa = \frac{a}{b}$, where a is the long radii of the nanoparticle and b is the short radii of the nanoparticle, as seen in figure 2.1b. $G(\kappa)$ is an aspect ratio dependent function defined as

$$G(\kappa) = \begin{cases} \frac{1}{2} + \frac{\kappa^2}{4\sqrt{1-\kappa^2}} \ln\left(\frac{1+\sqrt{1-\kappa^2}}{1-\sqrt{1-\kappa^2}}\right), & \text{if } \kappa \leq 1 \\ \frac{1}{2} + \frac{\kappa}{2\sqrt{1-\kappa^{-2}}} \arcsin(\sqrt{1-\kappa^{-2}}), & \text{if } \kappa > 1. \end{cases} \tag{2.9}$$

2.2 Nanoparticles at fluid interfaces

Nanoparticles may adsorb strongly at liquid-vapour interfaces. An adsorption energy ranging from 10 to $10^3 k_B T$ is estimated for nanoparticles [12]. The nanoparticles may form mono- or multilayers, which implies that an interface is completely covered by nanoparticles. Submonolayers of nanoparticles, implying less than full interface coverage, may result in aggregation, flocculation or self-assembly. Aggregation is the phenomenon where nanoparticles "clump together" creating clusters that are kinetically stable. Flocculation is the same phenomena as an aggregation, but less stable. A flocculation is easy to mix into an even distribution. Self-assembly is an aggregation in an organised and predictable way, and is possible if the forces between the nanoparticles depends on the orientation of the nanoparticle. It has been shown that prolate ellipsoidal nanoparticles exhibit orientation-dependent capillary forces [7,8], and may therefore self-assemble.

2.2.1 Wetting

The wetting of a nanoparticle is defined as the equilibrium position of the nanoparticle in relation to the liquid-vapour interface. In this context, the definition of the interface is somewhat unclear. A liquid-vapour interface is a two-dimensional entity to the human eye, but it is three-dimensional in the microscopic world. This is because the behaviour of atoms around an interface behaves differently from atoms in the bulk. The Gibbs dividing surface is for this reason introduced, and is defined as the inflection point of the phase density curve. The wetting l is calculated as distance from the nanoparticle centre of mass to the equilibrium position. By convention, a non-wetting nanoparticle will submerge completely in the vapour phase, a partially wetting nanoparticle will adsorb at the liquid-vapour interface, and a completely wetting nanoparticle will submerge completely in the liquid phase [2]. A partially wetting nanoparticle has a low wettability if the contact angle is $\theta > 90°$ and high wettability if it is $\theta < 90°$. The contact angle may be calculated using Young's equation or Young-Dupré's, as described in section 2.1. However, the solid-fluid interface tensions, γ_{sv} and, γ_{sl}, and the line tension, τ, are difficult to calculate. An easier approach is a strict geometrical consideration by calculating

$$\cos\theta = \frac{l}{R}, \tag{2.10}$$

where R is the radius of the spherical nanoparticle. For prolate ellipsoidal nanoparticles the nanoparticle has two unequal radii a and b. The contact angle, θ, is the same all around the three-phase line. The real contact angle of a prolate ellipsoidal nanoparticle is somewhere between the value found using equation 2.10 when inserting a and b for R.

Particles will move from the bulk phases to be adsorbed at a fluid interface if it reduces the free energy of the system. By inspecting equation 2.3, it is apparent that a nanoparticle will adsorb at the interface if the liquid-vapour interface tension, γ_{lv}, is high and the nanoparticle-fluid interface tensions, γ_{sl} and γ_{sv}, are low. The nanoparticle will effectively reduce the interface tension of the liquid-vapour interface by adsorbing to it, which is a common application of nanoparticles. For sufficiently small nanoparticles the line tension is a significant factor [13–16].

The size of the nanoparticle is an important factor to its stability. The free energy of spherical nanoparticles at interfaces, derived by Aveyard and Clint [10] as seen in equation 2.4, states that $\Delta F_{\text{int}} \propto R^2$. This means that a smaller nanoparticle will adsorb more strongly at a fluid interface compared to a large nanoparticle. The shape and orientation of the nanoparticle is also important in its stability. The free energy for ellipsoidal nanoparticles, derived by Faraudo and Bresme [17], is shown in equation 2.8. A prolate ellipsoidal nanoparticle laying flat on the interface will be less stable than a spherical nanoparticle, which again is less stable than an oblate ellipsoidal nanoparticle laying flat on the interface [9].

The density and temperature of the system are important for the wetting of nanoparticles. A two-phase system that is close to the triple point will have a diffuse interface with a high interface thickness. Conversely, a system with a low temperature will have a distinct interface with a low interface thickness. A high interface thickness is a result of low interface tension, and conversely a low interface thickness is a result of high interface tension. This means that a nanoparticle will adsorb more strongly to a thin interface compared to a thick interface, because this will give a larger difference in the effective liquid-vapour interface tension.

2.2.2 Brownian motion

Any nanoparticle in contact with a medium will move around in a random motion. This is known as Brownian motion, named after botanist Robert Brown. He observed that the pollen grains moved around, without currents or evaporation. It is now known that the movement of such nanoparticles is due to the random bombardment of the nanoparticle from the fluid particles that surrounds it. Einstein was the first to provide a theoretical analysis of Brownian motion [18].

In one dimension, Einstein's approach was: Let $x(t)$ be the position of the nanoparticle, and let $x(0) = 0$. After on average a time τ^* a collision occurs, and the particle jumps on average a distance Δx in either positive or negative direction. A jump in either direction is equally probable. The probability that the particle is at a position $x(t)$ after a time t is then equal to the probability, in a series of $n = \frac{t}{\tau^*}$ jumps, the particle makes $m = \frac{x}{\Delta x}$ more jumps in the positive direction than the negative direction. That is, it makes $\frac{1}{2}(n+m)$ jumps in the positive direction and $\frac{1}{2}(n-m)$ jumps in the negative direction. The probability is then given by the binomial expression,

$$p_n(m) = \frac{n!}{\left(\frac{1}{2}(n+m)\right)!\left(\frac{1}{2}(n-m)\right)!}\left(\frac{1}{2}\right)^n, \tag{2.11}$$

with the result that

$$\langle m \rangle = 0, \qquad \langle m^2 \rangle = n. \tag{2.12}$$

This means that for $t >> \tau^*$,

$$\langle x(t) \rangle = 0, \qquad \langle x^2(t) \rangle = \Delta x^2 \frac{t}{\tau^*}. \tag{2.13}$$

This is known as the mean-square displacement (MSD). For a nanoparticle adsorbed at a liquid-vapour interface, the two-dimensional mean-square displacement becomes,

$$MSD(t) = \langle (r(t) - r(0))^2 \rangle = 4Dt, \tag{2.14}$$

where $D = \frac{l^2}{2\tau^*}$ is the two-dimensional self-diffusion coefficient and $r^2(t) = y^2(t) + z^2(t)$.

2.2.3 Interface deformation

There are two types of interface deformations, fluctuation-induced deformations and static deformations. The fluctuation-induced deformations are caused by thermal fluctuations, while static interface deformations may be caused by a nanoparticle adsorbed at a liquid-vapour interface. The static interface deformation is a result of the weight, shape and wetting properties of the nanoparticle. The interface deformation as a result of the nanoparticle weight is insignificant for nanoparticles of radius $R < 5\,\mu\text{m}$ [19]. The interface will deform if the nanoparticle shape deviates from a sphere. For example, a prolate ellipsoidal nanoparticle flat on the interface with a contact angle $\theta \neq 90°$, as seen in figure 2.2a. This is because the fluid nanoparticles will adapt themselves in order to reduce the interfacial area and the three-phase line, which lowers the free energy. The fluid nanoparticles will adapt in order to establish the same contact angle, θ, along the three-phase line, which may be approximated with the Young-Dupré's equation as seen in equation 2.6. Δh is the maximum meniscus height of the deformation. For a prolate ellipsoidal nanoparticle flat on the interface, the interface deformation will be largest for contact angles between 40° and 55° [7, 8].

The pitch of a prolate ellipsoidal nanoparticle adsorbed at a fluid interface is defined as $\cos\phi = \boldsymbol{e}_i \cdot \boldsymbol{x}$, where $\boldsymbol{e}_i$ is the direction of the long axis of the prolate ellipsoidal nanoparticle and $\boldsymbol{x}$ is a vector perpendicular to the fluid interface. A prolate ellipsoidal nanoparticle that is tilted with pitches $\phi \neq 0$ and $\phi \neq \frac{\pi}{2}$ will cause deformations [5, 20], as seen in figure 2.2b.

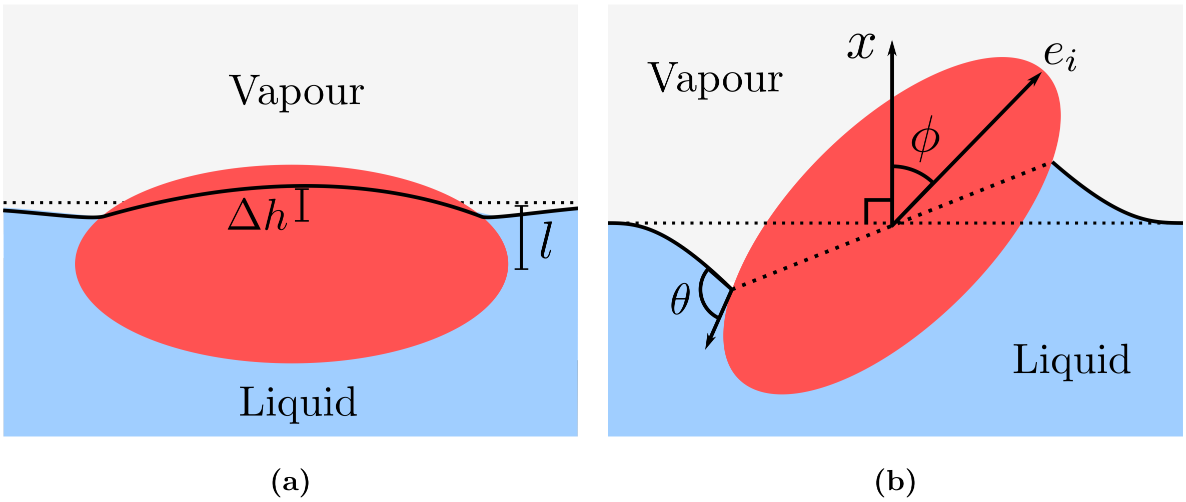

Figure 2.2: Side view of a prolate ellipsoidal nanoparticle adsorbed at a liquid-vapour interface inducing interface deformations. **(a)** A prolate ellipsoidal nanoparticle laying flat on the interface. Δh is the maximal meniscus height of the deformation and l is the distance from the nanoparticle centre to the interface position. **(b)** A prolate ellipsoidal nanoparticle that is tilted with pitch ϕ.

2.3 Forces acting on nanoparticles at fluid interfaces

The forces acting on nanoparticles adsorbed at fluid interfaces may be divided into two types, direct and indirect forces. Direct forces include for example van der Waals and electrostatic forces, which are also present in the bulk fluids. The van der Waals force is the only direct force that is included in this thesis. Indirect forces are mediated the presence of for example an interface or solvent particles.

2.3.1 Van der Waals force

The van der Waals force is omnipresent and is caused by a transient shift in electron density around an atom. It is the weakest of the chemical forces, ranging from approximately 0.1 to 1 k_BT for nanoparticles adsorbed at a liquid-vapour interface [9]. The van der Waals force between partially wetting nanoparticles is more complicated than nanoparticles submerged in bulk phases. The attractive part of the van der Waals force varies with d^{-6}, where d is the particle separation. It is predicted to be sensitive to solvent conditions. Williams and Berg [21] proposed a Hamaker constant for nanoparticles at liquid-vapour interfaces. It illustrated that the van der Waals force is expected to be stronger at the interface compared to the bulk phases. In computer simulations, the van der Waals force is modelled using the Lennard-Jones potential, and the direct

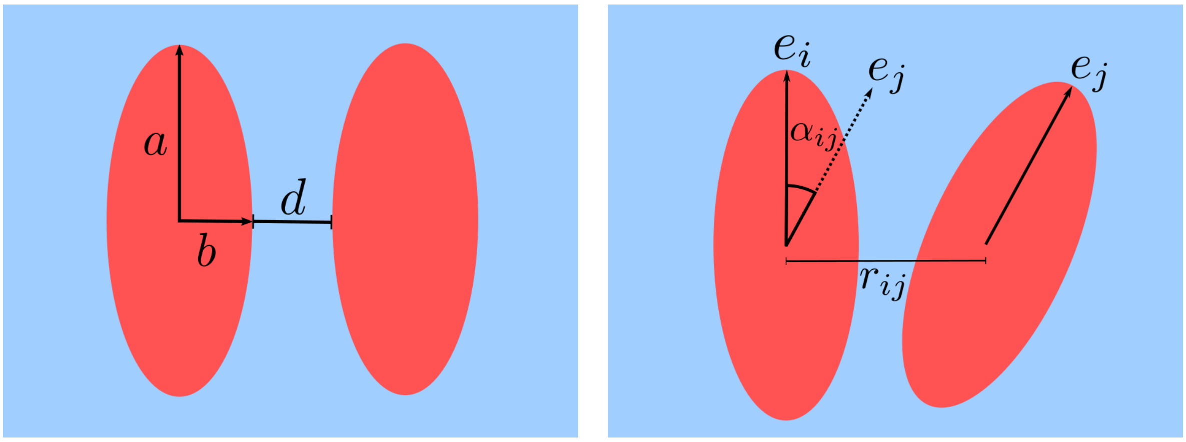

(a) **(b)**

Figure 2.3: **(a)** Top-down view of two prolate ellipsoidal nanoparticles adsorbed at a liquid-vapour interface. a and b are the radii of the nanoparticle, and d is the surface-to-surface distance. **(b)** Top-down view of two prolate ellipsoidal nanoparticles adsorbed to a liquid-vapour interface. The vectors $\boldsymbol{e}_i$ and $\boldsymbol{e}_j$ indicate the orientation of nanoparticle i and j respectively. α_{ij} is the angle between vector $\boldsymbol{e}_i$ and $\boldsymbol{e}_j$, and $\boldsymbol{r}_{ij}$ is the centre-to-centre nanoparticle separation.

nanoparticle-nanoparticle interaction is unchanged by the solvent.

2.3.2 Solvent-mediated forces

The solvent-mediated forces are the forces acting on a solute due to the surrounding solvent. As the nanoparticle size approaches the solvent size, the solvent-mediated forces are expected to get more pronounced. The depletion region is $d < \sigma_0$, where σ_0 is the solvent diameter and d is the nanoparticle-nanoparticle separation, as seen in figure 2.3a. The depletion force may be approximated with Derjaguin approximation.

Outside the depletion region, the solvent-mediated force will exhibit oscillations that decay. These oscillations are connected to the packing of solvent particles between the nanoparticles. The oscillations will produce peaks close to $d = n\sigma_0$, where n is a whole number. This is because there will be room for n solvent particles between two nanoparticles.

2.3.3 Capillary forces

The capillary force is caused by deformations of the interface, as discussed in section 2.2.3. The orientation of a prolate ellipsoidal nanoparticle adsorbed at a liquid-vapour

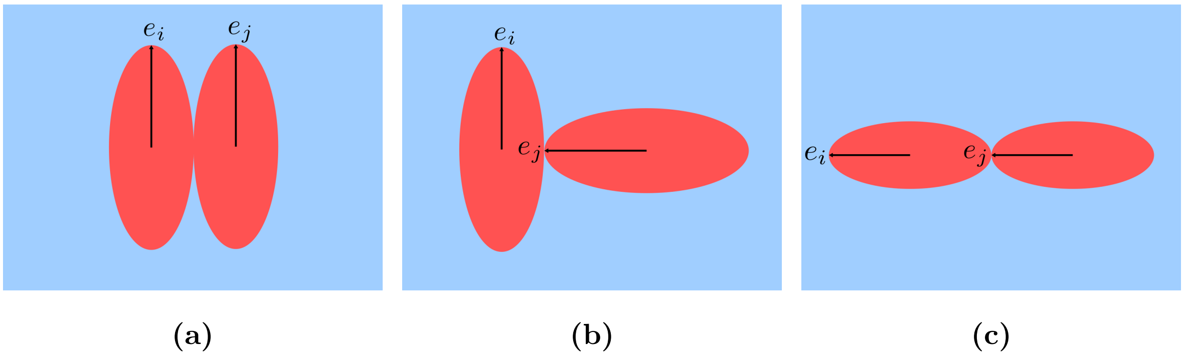

Figure 2.4: Top-down view of possible prolate-prolate configurations, **(a)** side-by-side, **(b)** tip-to-side and **(c)** tip-to-tip.

interface, as seen in figure 2.3b, is defined by the unit vector $\boldsymbol{e}_i$. The nanoparticle is symmetric, implying that there are two equivalent choices for $\boldsymbol{e}_i$. The angle between two nanoparticles is determined by $\cos\alpha_{ij} = \boldsymbol{e}_i \cdot \boldsymbol{e}_j$, where $\alpha_{ij} \in [0, \pi]$. The potential energy of two prolate ellipsoidal nanoparticles with a nanoparticle separation d as a result of the lateral capillary interaction energy is described as,

$$u_{\text{cap}}^{\text{quad}}(d, \alpha_{ij}) = -3\pi\gamma_{lv}\cos(2\alpha_{ij})\Delta h^2 \left(\frac{b}{d}\right)^4, \tag{2.15}$$

where Δh is the maximum meniscus height, γ_{lv} is the liquid and vapour interface tension and b is the short radius of the nanoparticle [7]. From this equation it is apparent that the nanoparticles are attractive for orientations $\alpha = 0$ and $\alpha = \pi$, and repulsive for orientation $\alpha = \frac{\pi}{2}$. The first case corresponds to the *side-by-side* or the *tip-to-tip* orientation while the second case corresponds to the *tip-to-side*, as seen in figure 2.4. The maximum meniscus height is predicted to be around $\frac{\Delta h}{b} = 0.1$ for nanoparticles of aspect ratio $\kappa = 2$ and contact angle $\theta = 50°$. The capillary interaction varies with d^{-4}, which implies that it is quite long range.

Chapter 3

Methodology

This chapter presents the molecular dynamics method for modelling prolate ellipsoidal nanoparticles and spherical fluid particles used in this thesis. Details for each simulation are also presented.

3.1 Molecular dynamics simulation

Molecular dynamics simulation is a N-body simulation method used to study the movements of atoms. This is done by solving Newton's second law of motion,

$$\boldsymbol{f}_i(\boldsymbol{r}_i) = m_i \frac{d^2\boldsymbol{r}_i}{dt^2}, \tag{3.1}$$

where $\boldsymbol{f}_i$ is the force acting on the centre of mass of particle i, $\boldsymbol{r}_i$ is the position of the centre of mass of particle i, m_i is the mass of particle i, and t is time. The force is determined by,

$$\boldsymbol{f}_i(\boldsymbol{r}_i) = -\sum_{\substack{j=1 \\ j\neq i}}^{N-1} \frac{\partial U_{ij}}{\partial \boldsymbol{r}_{ij}}, \tag{3.2}$$

where U_{ij} is the potential energy of particle i due to particle j, and $\boldsymbol{r}_{ij} = \boldsymbol{r}_i - \boldsymbol{r}_j$ is a vector conjoining the centre of particle i and j. There are many possible choices for the force field $\boldsymbol{U}_{ij}(\boldsymbol{r}_{ij})$, depending on the type of atoms and molecules involved.

Equation 3.1 is solved using a finite difference method. The Velocity Verlet integration algorithm [22] is used in this work,

1. Calculate $\boldsymbol{v}_i(t + \Delta t/2) = \boldsymbol{v}_i(t) + \frac{1}{2}\boldsymbol{a}_i(t)\Delta t$,

2. Calculate $\boldsymbol{r}_i(t + \Delta t) = \boldsymbol{r}_i(t) + \boldsymbol{v}_i(t + \Delta t/2)\Delta t$,

3. Derive $\boldsymbol{a}_i(t+\Delta t) = \dfrac{1}{m}\boldsymbol{f}_i(\boldsymbol{r}_i(t+\Delta t))$,

4. Calculate $\boldsymbol{v}_i(t+\Delta t) = \boldsymbol{v}_i(t+\Delta/2) + \dfrac{1}{2}\boldsymbol{a}_i(t+\Delta t)\Delta t$,

where Δt is the time step, and $\boldsymbol{v}_i$ and $\boldsymbol{a}_i$ are the velocity and the acceleration of particle i, defined as

$$\boldsymbol{v}_i(t) \equiv \frac{d\boldsymbol{r}_i}{dt}, \qquad \boldsymbol{a}_i(t) \equiv \frac{d^2\boldsymbol{r}_i}{dt^2}. \tag{3.3}$$

3.1.1 Non-spherical particles

Non-spherical particles add a new layer of complexity to the problem, namely rotation. Up until 1977, when Evans and Murad [23] suggested a new algorithm, the Euler angles, (ϕ, θ, ψ), were used in some variation to describe the orientation of particles. The problem with this is that the sine and cosine of the Euler angles are computationally expensive and they produce singularities in the equations of motion whenever they approach zero, which causes instability. This is generally unwanted, and Evans and Murad suggested an elegant solution using quaternions,

$$\boldsymbol{Q}_i = \begin{pmatrix} q_0 & q_1 & q_2 & q_3 \end{pmatrix}, \tag{3.4}$$

where each quaternion is related to the Euler angles,

$$\begin{aligned} q_0 &= \cos\tfrac{1}{2}\theta\cos\tfrac{1}{2}(\phi+\psi), \\ q_1 &= \sin\tfrac{1}{2}\theta\cos\tfrac{1}{2}(\phi-\psi), \\ q_2 &= \sin\tfrac{1}{2}\theta\sin\tfrac{1}{2}(\phi-\psi), \\ q_3 &= \cos\tfrac{1}{2}\theta\sin\tfrac{1}{2}(\phi+\psi). \end{aligned} \tag{3.5}$$

The quaternions are not independent, but satisfy the relation $q_0^2 + q_1^2 + q_2^2 + q_3^2 = 1$. If this constraint is satisfied at time zero, it will be satisfied for every subsequent timestep. However, because the equations of motion are not solved exactly, the constraint will only be approximately satisfied. This is solved by rescaling the quaternions whenever the constraint is not satisfied. The rotation matrix $\mathbb{A}_i$ describes the rotation of any vector $\boldsymbol{u}_i$ from the space-fixed to body-fixed frame,

$$\boldsymbol{u}_i^b = \mathbb{A}_i\boldsymbol{u}_i^s, \tag{3.6}$$

where $\boldsymbol{u}_i^s$ and $\boldsymbol{u}_i^b$ are space-fixed and body-fixed frames, respectively. The space-fixed frame is a vector in relation to the simulation box, while the body-fixed frame is a vector in relation to the particle. The rotation matrix is constructed from the quaternions,

$$\mathbb{A}_i = \begin{pmatrix} q_0^2+q_1^2-q_2^2-q_3^2 & 2(q_1q_2-q_3q_0) & 2(q_2q_0+q_1q_3) \\ 2(q_1q_2+q_3q_0) & q_0^2-q_1^2+q_2^2-q_3^2 & 2(q_1q_3-q_1q_0) \\ 2(q_1q_3-q_2q_0) & 2(q_2q_3+q_1q_0) & q_0^2-q_1^2-q_2^2+q_3^2 \end{pmatrix}. \tag{3.7}$$

The torque $\boldsymbol{\tau}_i$ is determined in terms of the angular velocity $\boldsymbol{\omega}_i$ and the moment of inertia $\boldsymbol{I}_i$,

$$\boldsymbol{\tau}_i = \boldsymbol{I}_i \frac{d\boldsymbol{\omega}_i}{dt}. \tag{3.8}$$

This equation may be solved using a finite difference method, equivalent to the Velocity Verlet algorithm for equation 3.1 discussed in section 3.1. The torque is determined in terms of the force field,

$$\boldsymbol{\tau}_i(\mathbb{A}_i) = -\sum_{m=1}^{3} \boldsymbol{a}_{i,m} \times \frac{\partial \boldsymbol{U}_i}{\partial \boldsymbol{a}_{i,m}}, \tag{3.9}$$

where $\boldsymbol{a}_{i,m}$ is the m-th row of the rotation matrix $\mathbb{A}_i$ and $\boldsymbol{U}_i$ is the force field acting on particle i [24]. In this case, the force field is a function of the rotation matrix, $\mathbb{A}_i$, and the position, $\boldsymbol{r}_i$. The angular velocities are related to the quaternions by [25],

$$\frac{\partial \boldsymbol{Q}_i^T}{\partial t} = \frac{1}{2} \begin{pmatrix} q_0 & -q_1 & -q_2 & -q_3 \\ q_1 & q_0 & -q_3 & q_2 \\ q_2 & q_3 & q_0 & -q_1 \\ q_3 & -q_2 & q_1 & q_0 \end{pmatrix} \begin{pmatrix} 0 \\ \omega_x^b \\ \omega_y^b \\ \omega_z^b \end{pmatrix}. \tag{3.10}$$

3.1.2 Force fields

The Lennard-Jones potential is a common force field for atoms governed by van der Waals forces,

$$U_{ij}(\|\boldsymbol{r}_{ij}\|) = 4\epsilon_{ij} \left(\left(\frac{\sigma_{ij}}{\|\boldsymbol{r}_{ij}\|} \right)^{12} - \left(\frac{\sigma_{ij}}{\|\boldsymbol{r}_{ij}\|} \right)^{6} \right), \tag{3.11}$$

where U_{ij} is the potential energy of particle i as a result of all other particles j, $\|\boldsymbol{r}_{ij}\|$ is the Euclidean norm of $\boldsymbol{r}_{ij}$, σ_{ij} is the size of the particle, and ϵ_{ij} is the depth of the energy well. The potential consists of a repulsive term, $\|\boldsymbol{r}_{ij}\|^{-12}$, and an attractive term, $\|\boldsymbol{r}_{ij}\|^{-6}$. Whenever $\|\boldsymbol{r}_{ij}\| > r_c$, the potential energy is set to zero. This reduces the amount of calculations needed.

The force on particle i as a consequence of the potential energy, in context with equation 3.2, is

$$\boldsymbol{f}_i(\boldsymbol{r}_i) = \sum_{\substack{j=1\\j\neq i}}^{N-1} 24\epsilon_{ij}\frac{\boldsymbol{r}_{ij}}{\|\boldsymbol{r}_{ij}\|}\left(2\left(\frac{\sigma_{ij}^{12}}{\|\boldsymbol{r}_{ij}\|^{13}}\right)-\left(\frac{\sigma_{ij}^{6}}{\|\boldsymbol{r}_{ij}\|^{7}}\right)\right). \tag{3.12}$$

To model ellipsoidal particles, the Lennard-Jones potential is not sufficient. An alternative is the Gay-Berne potential introduced by Gay and Berne [26] in 1981. The modified Gay-Berne potential as described by Evaraers and Ejtehadi [27,28] is defined as a product of three terms,

$$U_i(\mathbb{A}_i, \boldsymbol{r}_i) = \sum_{\substack{j=1\\j\neq i}}^{N-1} U_r(\mathbb{A}_i, \mathbb{A}_j, \boldsymbol{r}_{ij})\eta_{ij}(\mathbb{A}_i, \mathbb{A}_j)\chi_{ij}(\mathbb{A}_i, \mathbb{A}_j, \hat{\boldsymbol{r}}_{ij}), \tag{3.13}$$

where U_r controls the distance dependence and has the form of the Lennard-Jones potential. η and χ control the interaction strength as a function of relative orientation and position. $\mathbb{A}_i$ is the rotation matrix that describes the orientation of particle i. $\hat{\boldsymbol{r}}_{ij} = \frac{\boldsymbol{r}_{ij}}{\|\boldsymbol{r}_{ij}\|}$ is the unit distance vector. U_r is defined as

$$U_r(\mathbb{A}_i, \mathbb{A}_j, \boldsymbol{r_{ij}}) = 4\epsilon_{ij}\left(\left(\frac{\sigma_{ij}}{h_{ij}+\gamma\sigma_{ij}}\right)^{12} - \left(\frac{\sigma_{ij}}{h_{ij}+\gamma\sigma_{ij}}\right)^{6}\right). \tag{3.14}$$

$h_{ij} = \min(|\boldsymbol{r}_i - \boldsymbol{r}_j|)$ is the minimum distance between the surface of particle i and j, ϵ_{ij} is the well depth, $\min(U_r) = -\epsilon_{ij}$, and γ is a shift parameter. h'_{ij} is the Perram approximation of h_{ij} determined by

$$h'_{ij} = \|\boldsymbol{r}_{ij}\| - \sigma_{ij}(\mathbb{A}_i, \mathbb{A}_j, \hat{\boldsymbol{r}}_{ij}), \tag{3.15}$$

where

$$\sigma_{ij}(\mathbb{A}_i, \mathbb{A}_j, \hat{\boldsymbol{r}}_{\boldsymbol{ij}})) = \left(\frac{1}{2}\hat{\boldsymbol{r}}_{\boldsymbol{ij}}{}^T\mathbb{G}_{ij}^{-1}(\mathbb{A}_i, \mathbb{A}_j)\hat{\boldsymbol{r}}_{\boldsymbol{ij}}\right)^{-\frac{1}{2}}, \tag{3.16}$$

$$\mathbb{G}_{ij}(\mathbb{A}_i, \mathbb{A}_j) = \mathbb{A}_i^T\mathbb{S}_i^2\mathbb{A}_i + \mathbb{A}_j^T\mathbb{S}_j^2\mathbb{A}_j, \tag{3.17}$$

$$\mathbb{S}_i = \begin{pmatrix}\sigma_x & 0 & 0\\ 0 & \sigma_y & 0\\ 0 & 0 & \sigma_z\end{pmatrix}. \tag{3.18}$$

$\mathbb{S}_i$ is the size matrix and σ_x, σ_y and σ_z are the diameters of the ellipsoid [29]. The Perram approximation in equation 3.15 fails if any of the diagonal elements of $\mathbb{S}_i$ is much larger than σ_{ij}. This occurs when a large particle interacts with a small particle, or when the tip of a long particle interacts with the side of another long particle. η_{ij} is determined by

$$\eta_{ij}(\mathbb{A}_i, \mathbb{A}_j) = \left(\frac{2 s_i s_j}{\det[\mathbb{G}_{ij}(\mathbb{A}_i, \mathbb{A}_j)]} \right)^{\frac{\upsilon}{2}}, \tag{3.19}$$

$$s_i = (a_i b_i + c_i^2)\sqrt{a_i b_i}, \tag{3.20}$$

where υ is an empirical constant. χ is determined by

$$\chi_{ij}(\mathbb{A}_i, \mathbb{A}_j, \hat{\boldsymbol{r}}_{ij}) = (2 \hat{\boldsymbol{r}}_{ij}^T \mathbb{B}_{ij}^{-1}(\mathbb{A}_i, \mathbb{A}_j) \hat{\boldsymbol{r}}_{ij})^{\mu}, \tag{3.21}$$

$$\mathbb{B}_{ij}(\mathbb{A}_i, \mathbb{A}_j) = \mathbb{A}_i^T \mathbb{E}_i \mathbb{A}_i + \mathbb{A}_j^T \mathbb{E}_j \mathbb{A}_j, \tag{3.22}$$

$$\mathbb{E}_i = \begin{pmatrix} e_{ai}^{-1/\mu} & 0 & 0 \\ 0 & e_{bi}^{-1/\mu} & 0 \\ 0 & 0 & e_{ci}^{-1/\mu} \end{pmatrix}, \tag{3.23}$$

where e_{ai}, e_{bi} and e_{ci} are the relative well depth for side-to-side, face-to-face and end-to-end interactions between two ellipsoids of type i, respectively, and μ is an empirical constant. The equations for the force and torque for the Gay-Berne potential are reported by Allen and Germano [24].

3.1.3 Reduced units

Reduced units are used in molecular dynamics simulations to make the implementation and control of the program easier. Real quantities are defined in terms of the fundamental quantities mass m_0, distance σ_0, energy ϵ_0, and the Boltzmann constant k_B. The reduced units are denoted with a superscript asterisk, *e.g.* x^*. The real quantities can be found by inserting the values of m_0, σ_0, and ϵ_0 for a specific material. The definition of the reduced units are shown in table 3.1.

3.1.4 Thermostat

When molecular dynamics simulations are performed in the canonical ensemble it means that the number of particles N, the volume V and the temperature T are kept constant. The number of particles and the volume are simple to keep constant. However, a thermostat is needed to keep the temperature constant. The Nosé-Hoover [30] thermostat was used in this work.

Table 3.1: Definition of Lennard-Jones reduced units

Physical quantity	Symbol	Definition of reduced unit
Mass	m	$m^* = \frac{m}{m_0}$
Distance	x	$x^* = \frac{x}{\sigma_0}$
Time	t	$t^* = t\tau = t\left(\frac{\epsilon_0}{m_0\sigma_0^2}\right)^{1/2}$
Temperature	T	$T^* = \frac{k_B T}{\epsilon_0}$
Pressure	P	$P^* = P\frac{\sigma_0^3}{\epsilon_0}$
Energy	E	$E^* = \frac{E}{\epsilon_0}$
Force	f	$f^* = f\frac{\sigma_0}{\epsilon_0}$
Velocity	v	$v^* = \frac{v\tau}{\sigma_0}$
Number density	n	$n^* = n\sigma_0^3$
Density	ρ	$\rho^* = \rho\frac{\sigma_0^3}{m_0}$
Surface tension	γ	$\gamma^* = \gamma\frac{\sigma_0^2}{\epsilon_0}$

3.1.5 Periodic boundaries

Periodic boundary conditions imply that whenever a particle cross the boundary of the simulation cell, a copy of the particle enters the other side of the simulation cell. This makes it possible to approximate an infinite system, and it is thus possible to get closer to the thermodynamic limit while keeping the computational cost low. A small number of atoms in the system may be related to finite-size effects, and should be avoided at all cost.

3.2 Simulation details

Molecular dynamics simulations in the canonical (NVT) ensemble were performed to model prolate ellipsoidal nanoparticles adsorbed at a liquid-vapour interface. Canonical (NVT) ensemble implies that the number of particles N, the volume V, and the temperature T are kept constant. The size of the simulation box was varied depending on the simulation case. A typical size used was $L = [68.4\sigma_0, 34.2\sigma_0, 34.2\sigma_0]$ with 32000 fluid particles. The timestep was set to $\Delta t^* = 0.002$.

The simulations were preformed using LAMMPS[1] (Large-scale Atomic/Molecular

---

[1] http://lammps.sandia.gov/

Massively Parallel Simulator), which is a software for molecular dynamics simulations developed by Sandia National Laboratories [31].

3.2.1 Force fields

The fluid-fluid interaction was modelled using the Lennard-Jones potential. The diameter was set to $\sigma_{ff} = \sigma_0$, the well depth to $\epsilon_{ff} = \epsilon_0$ and the cut-off to $r_{ff} = 3.0\sigma_0$ for all simulation cases.

The nanoparticle-fluid interaction was modelled using the Gay-Berne potential. Five different nanoparticle sizes were considered,

(a) radii $a = 7.5\sigma_0, b = c = 2.5\sigma_0$, aspect ratio $\kappa = 3$,

(b) radii $a = 5.0\sigma_0, b = c = 2.5\sigma_0$, aspect ratio $\kappa = 2$,

(c) radii $a = b = c = 2.5\sigma_0$, aspect ratio $\kappa = 1$,

(d) radii $a = 4.5\sigma_0, b = c = 1.5\sigma_0$, aspect ratio $\kappa = 3$, and

(e) radii $a = 1.5\sigma_0, b = c = 0.5\sigma_0$, aspect ratio $\kappa = 3$.

This corresponds approximately to nanoparticle diameters ranging from 0.3 nm to 5.0 nm. These nanoparticle sizes were chosen to explore the significance of nanoparticle size and aspect ratio.

The relative well depths for side-to-side, face-to-face and end-to-end is the relative potential energy minima between particles when approaching each other from side-to-side, face-to-face and end-to-end, respectively. For the fluid particles, the well depth was equal all around the particle, meaning $e_{af} = e_{bf} = e_{cf} = 3\sigma_0$, as suggested by other works [32–34]. Two well depth ratios $\kappa' = \frac{e_{ap}}{e_{bp}} = \frac{e_{ap}}{e_{cp}}$ were considered for the nanoparticle,

(a) well depth ratios $\kappa' = 5$, $e_{ap} = 0.2\epsilon_0$, $e_{bp} = e_{cp} = \epsilon_0$ and

(b) well depth ratios $\kappa' = 1$, $e_{ap} = e_{bp} = e_{cp} = \epsilon_0$.

The well depth ratio (a) is suggested by other works to be a good coarse-grained approximation of liquid crystal molecules [32–34]. The equal well depth ratio (b) was used to compare the results from continuum studies [5, 8, 20]. Spherical nanoparticles were only studied with a well depth ratio $\kappa' = 1$. The potential as a function of

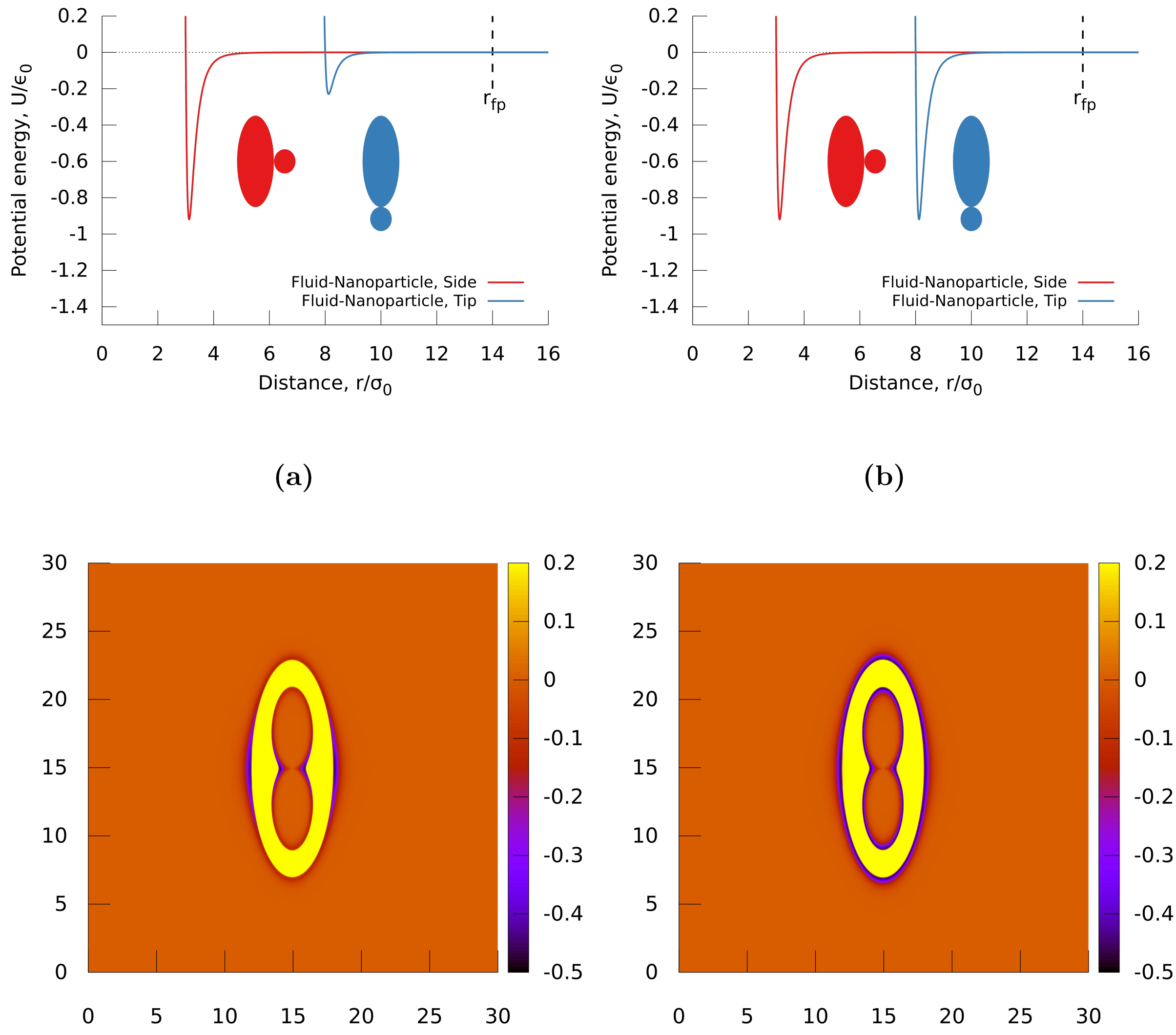

(a) **(b)**

(c) **(d)**

Figure 3.1: The potential energy between a fluid particle and a nanoparticle of radii $a = 7.5\sigma_0, b = c = 2.5\sigma_0$ and well depth $\epsilon_{fp} = 3\epsilon_0$, and relative well depth ratios **(a, c)** $\kappa' = 5$ and **(b, d)** $\kappa' = 1$. The well depth ϵ_{fp} does not correspond to the real energy minimum. See text for details.

nanoparticle separation for the different and equal well depth ratios is shown in figure 3.1 for a nanoparticle of radii $a = 7.5\sigma_0, b = c = 2.5\sigma_0$ and well depth $\epsilon_{fp} = 3\epsilon_0$.

The well depth, ϵ_{fp}, was varied depending on the degree of wetting wanted. The well depth ϵ_{fp} does not necessarily equal the real well depth, because of how the Gay-Berne potential is constructed. The real well depth decreases relative to the well depth ϵ_{fp} when the nanoparticle size increases. The potential energy as a function of nanoparticle separation with well depth $\epsilon_{fp} = 3\epsilon_0$ and of radii $a = 5\sigma_0, b = c = 2.5\sigma_0$ and $a = 7.5\sigma_0, b = c = 2.5\sigma_0$ is shown in figures 3.2a and 3.2b. This shows that the real well

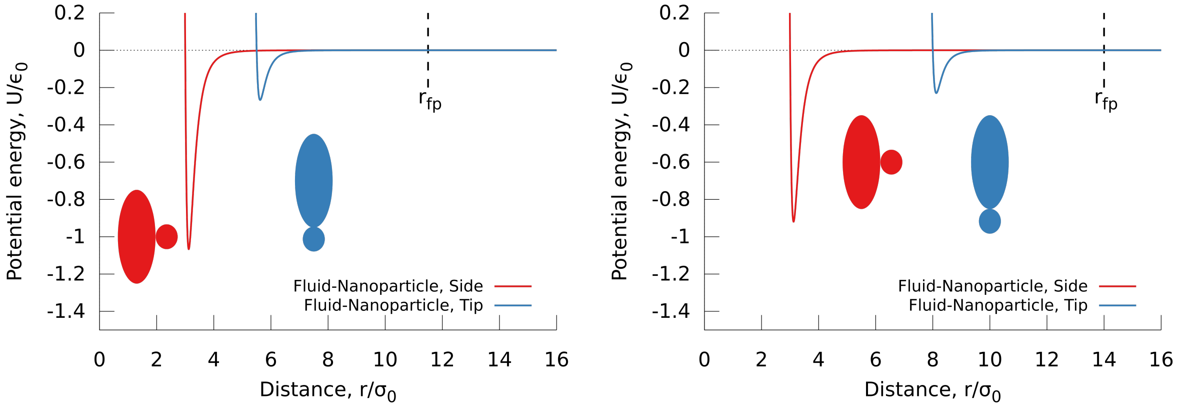

(a) **(b)**

Figure 3.2: Potential energy of the fluid-nanoparticle interaction for a nanoparticle with well depth $\epsilon_{fp} = 3\epsilon_0$ and of radii **(a)** $a = 5\sigma_0, b = c = 2.5\sigma_0$, and **(b)** $a = 7.5\sigma_0, b = c = 2.5\sigma_0$.

depth does not equal ϵ_{fp} and that the well depth is greater for radii $a = 5\sigma_0, b = c = 2.5\sigma_0$ compared to radii $a = 7.5\sigma_0, b = c = 2.5\sigma_0$.

The diameter of the fluid was set to $\sigma_{f,x} = \sigma_{f,y} = \sigma_{f,z} = \sigma_0$. As mentioned earlier, the Perram approximation fails if the size of the nanoparticle is much larger than the size of the fluid. This may be circumvented when there is no nanoparticle-nanoparticle interaction, by setting the diameter of the nanoparticle to

$$\sigma_{p,i} = \sqrt{\frac{(\sigma'_{p,i} + \sigma_{f,i})^2}{2} - \sigma_{f,i}^2}. \tag{3.24}$$

$\sigma_{p,i}$ is the input diameter of the nanoparticle in the Gay-Berne model, $\sigma'_{p,i}$ is the perceived diameter by the fluid and $\sigma_{f,i}$ is the diameter of the fluid. This does not give the correct nanoparticle size for the nanoparticle-nanoparticle interaction. The parameter σ_{fp} may be considered as the well width of the Gay-Berne potential, and was set to $\sigma_{fp} = \sigma_0$. The shift parameter and the empirical exponents were set to $\gamma = \upsilon = \mu = 1$ for all simulation cases.

Summary of force field parameters

Five different particle sizes with two different well depth ratios κ' were considered. Spherical nanoparticles were only considered with a well depth ratio $\kappa' = 1$. This sums up to a total of 9 different potentials. A complete list of force field parameters and graphs of potential energy as a function of distance and orientation is presented in appendix A.

3.2.2 Comparison with a Lennard-Jones crystals

A face-centred cubic crystal of Lennard-Jones nanoparticles was placed in a prolate ellipsoidal shape. The diameter of the Lennard-Jones particles was set to $\sigma = \sigma_0$, the radii of the prolate ellipsoidal nanoparticle were set to $a = 7.5\sigma_0, b = c = 2.5\sigma_0$, and the lattice parameter of the crystal was set to $\frac{2^{1/6}}{\sqrt{2}}\sigma_0$. The crystal consisted of 181 nanoparticles, which corresponds to a density $\rho^* = 0.9218$. The potential energy of a fluid particle of diameter $\sigma = \sigma_0$ was calculated as it approached the crystal from the side and from the tip.

3.2.3 Two-phase system

A phase diagram of a Lennard-Jones fluid, as reported in several works [35, 36], may be studied to produce a two-phase system consisting of a liquid phase and a gas phase.

A two-phase system was created by placing a face-centred cubic structure of fluid particles with a density $\rho^* = 0.8$, with vacuum on each side equal to the volume of the face-centred cubic crystal. The size of the simulation box was varied depending on the size and amount of nanoparticles. The temperature was set to $T^* = 2.0$ for 5×10^3 timesteps to melt the crystal, and the temperature was subsequently reduced to $T^* = 0.7$ for the rest of the simulation. While the crystal was melting, the fluid particles were restricted to the initial crystal size. When the temperature was reduced the box increased on both sides in the x-direction. A two-phase system of liquid and vapour was formed after 15×10^3 timesteps of equilibration. The density profile of the two-phase system was curve fitted with

$$\rho(x) = \frac{1}{2}(\rho_l + \rho_v) - \frac{1}{2}(\rho_l - \rho_v)\tanh\left(\frac{x - x_e}{w}\right), \tag{3.25}$$

where ρ_l and ρ_v are the densities of the liquid and vapour phases, respectively, x_e is the position of the Gibbs dividing surface, and w is the width of the interface [25, 37]. The liquid-vapour interface tension, γ_{lv}, was calculated as described by Kirkwood and Buff,

$$\gamma_{lv} = \int_{x_l}^{x_v} [P_N(x) - P_T(x)]dx, \tag{3.26}$$

where the liquid-vapour interface is normal to the x-axis. x_v and x_l are positions in the vapour and liquid phases, respectively, and P_N and P_T are the normal and tangential pressure tensors, respectively [38].

3.2.4 Wetting

A two-phase system was created as described in section 3.2.3, and one nanoparticle was placed on the liquid-vapour interface. The nanoparticle was equilibrated on the surface for 10^3 timesteps. The mean distance from the nanoparticle centre of mass to the interface position as a function of the well depth, ϵ_{fp}, was calculated. The mean wetting, $\langle l \rangle$, was calculated for 5×10^5 timesteps. The wetting l/b is linear in the region $l/b \in [-1, 1]$. The linear regression was calculated, and was used in later simulations to choose the well depth, ϵ_{fp}, corresponding to the wanted wetting, l/b.

The pitch, ϕ, of the nanoparticle was calculated for various values of ϵ_{fp} and nanoparticle sizes. The pitch was calculated as $\cos\phi = \boldsymbol{e}_i \cdot \boldsymbol{x}$, where $\boldsymbol{x}$ is a unit vector normal to the liquid-vapour interface and $\boldsymbol{e}_i$ is a unit vector parallel to the long axis of the nanoparticle.

3.2.5 Brownian motion

One nanoparticle was placed at the liquid-vapour interface of a two-phase system, as described in section 3.2.3. The nanoparticle was equilibrated for 10^3 timesteps, and the position and orientation were then calculated for 5×10^6 timesteps. The mean-square displacement curve, as discussed in section 2.2.2, will have considerable amount of noise because there is only one nanoparticle in the simulation. This was avoided by running the simulation for many timesteps and splitting the run into blocks. Each block may be considered as an individual nanoparticle. The Brownian motion was investigated for a nanoparticle of radii $a = 7.5\sigma_0, b = c = 2.5\sigma_0$ and $a = b = c = 2.5\sigma_0$ for different wettabilities.

3.2.6 Interface deformation

A two-phase system was created as described in section 3.2.3, and one nanoparticle was placed at the liquid-vapour interface. The nanoparticle was equilibrated on the surface for 10^3 timesteps. The nanoparticle position and orientation were then fixed, while the local density of solvent nanoparticles was calculated in a slab around the nanoparticle for 5×10^5 timesteps. The slab had a thickness equal to the short diameter of the nanoparticle, $2b$, and was centred on the nanoparticle. The deformation was investigated for nanoparticle radii $a = 7.5\sigma_0, b = c = 2.5\sigma_0$ and $a = 5.0\sigma_0, b = c = 2.5\sigma_0$ for well depth ratios $\kappa' = 5$ and $\kappa' = 1$.

3.2.7 Solvent-mediated forces

A two-phase system was created as described in section 3.2.3, and a nanoparticle pair with a fixed separation d was placed at the liquid-vapour interface, as seen in figure 2.3a. The direct nanoparticle-nanoparticle interaction was turned off and the nanoparticle pair was modelled as a single rigid body. This implies that the force on each nanoparticle is summed up and added to both particles as a single body. The orientation of each nanoparticle was fixed in relation to each other, and the plane of the nanoparticle pair was fixed to be parallel to the liquid-vapour interface. The well depth, ϵ_{fp}, was chosen on the basis of the linear regression calculated in section 3.2.4. The force was calculated as,

$$f(d) = \frac{1}{2}\langle \boldsymbol{r}_{ij} \cdot (\boldsymbol{f}_i - \boldsymbol{f}_j)\rangle, \tag{3.27}$$

where $\boldsymbol{f}_i$ was the force acting on nanoparticle i and $\boldsymbol{r}_{ij}$ was the unit vector joining nanoparticle i and j. This implies that a negative force, $f(d)$, corresponds to an attractive force between the nanoparticles. The force was also calculated for nanoparticle pairs submerged in bulk liquid and gas. The bulk densities are tuned to have the same density as the two-phase system. The nanoparticles were equilibrated for 10^3 timesteps, and the force was calculated for 5×10^5 timesteps. One simulation was run for each separation d. LAMMPS simulation scripts are presented in appendix B.

3.3 Estimating errors

The mean of a property A is calculated as an arithmetic mean,

$$\langle A \rangle = \frac{1}{n}\sum_{i=0}^{n} A_i, \tag{3.28}$$

where n is the number of timesteps. The variance of A is calculated as,

$$\sigma_A^2 = \frac{1}{n-1}\sum_{i=0}^{n}(A_i - \langle A \rangle)^2. \tag{3.29}$$

where σ_A is the standard deviation. A molecular dynamics simulation consists of many timesteps, and each consecutive timestep is highly correlated. The system will relax after a certain number of steps, and a new calculation of A may be done. This time is known as the correlation time, and is the minimum amount of timesteps between each calculation of property A that does not result in correlated values. The correlation time may be found by block analysis. The array A is divided into n blocks of length n_b, totalling $b = nn_b$. For each block the mean and variance is calculated,

$$\langle A \rangle_b = \frac{1}{n_b} \sum_{i=0}^{n_b} A_i, \qquad \sigma^2_{A_b} = \frac{1}{n_b} \sum_{i=0}^{n_b} (A_i - \langle A \rangle_b)^2. \tag{3.30}$$

The statistical inefficiency may then be calculated as,

$$s = \lim_{t_b \to \infty} \frac{t_b \sigma^2_{A_b}}{\sigma^2_A}. \tag{3.31}$$

The statistical inefficiency s is plotted as a function of $\sqrt{t_b}$. The graph will show a steep rise and the give a plateau at high t_b. The plateau value is the correlation time of the system.

The variance of the mean of A is calculated as

$$\sigma^2_{\langle A \rangle} = \frac{1}{(n-1)n} \sum_{i=0}^{n} (A_i - \langle A \rangle)^2. \tag{3.32}$$

Chapter 4

Results and discussion

This chapter presents and discusses the results of the computations as explained in chapter 3.

4.1 Comparison with a Lennard-Jones crystal

The physical interpretation of a Gay-Berne prolate ellipsoidal nanoparticle is unclear, and the Gay-Berne potential was therefore compared to a Lennard-Jones crystal. The potential energy of a fluid particle as it approaches a prolate ellipsoidal Lennard-Jones crystal was calculated. A face-centred cubic crystal, as seen in figure 4.1a, was considered.

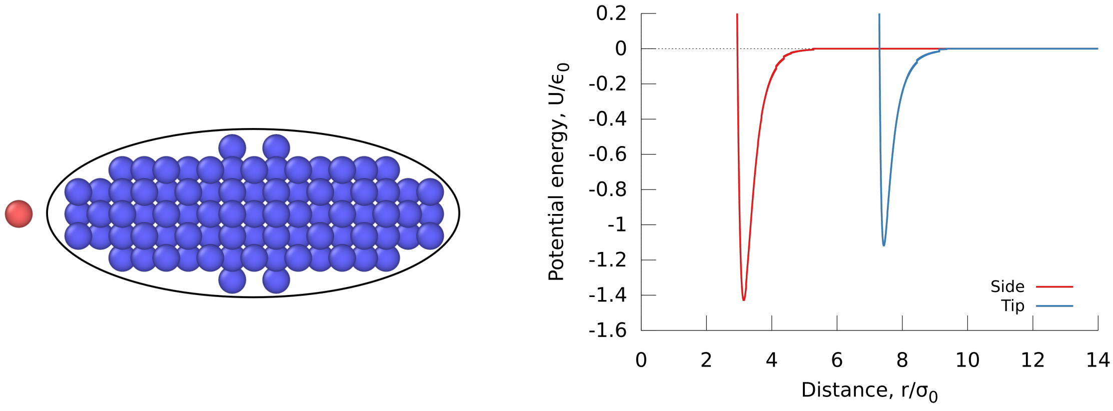

(a) (b)

Figure 4.1: **(a)** Snapshot of a fluid particle in red and a prolate ellipsoidal face-centred cubic crystal in blue. A prolate ellipsoid was superimposed over the crystal. **(b)** The potential energy of a fluid particle as a function of the distance between a fluid particle and the tip and side of a prolate ellipsoid face-centred cubic crystal consisting of Lennard-Jones particles.

The potential energy of the fluid particle as it approaches the crystal from the side and the tip is shown in figure 4.1b. The potential energy minimum when the fluid particle approaches the crystal was found to be $\min(U_{\text{side}}) = -1.43\epsilon_0$ and $\min(U_{\text{tip}}) = -1.12\epsilon_0$ when approaching the side and tip, respectively. This gives a well depth ratio of $\kappa' = 1.28$. The potential energy minimum of the side of the crystal was greater compared to the tip of the crystal. This is because more crystal particles may reach the fluid particle when approaching the side compared to approaching the tip. As the crystal size increases the well depth ratio is expected to approach one. This is because the interaction between the fluid and crystal will be more like an interaction between a fluid and a planar wall for both the fluid-tip and fluid-side interaction.

If the Lennard-Jones crystal was constructed of smaller particles the well depth ratio κ' would be larger. This is because the curvature on the tip of the crystal would be higher. Figure 4.1a shows the face-centred cubic crystal with a prolate ellipsoid superimposed. The crystal deviates from a prolate ellipsoid due to the roughness of the crystal curve, making it flat on the tip. However, the physical understanding of a crystal consisting of smaller particles is unclear. If the fluid particle is considered to be an argon atom, the particles of the crystal can not be significantly smaller than the fluid particle.

This suggests that a $\kappa' = 5$ is a high well depth ratio for a nanoparticle of radii $a = 7.5\sigma_0, b = c = 2.5\sigma_0$, if the model is designed to be a coarse-grained model of Lennard-Jones crystals. Babadi *et al.* [32] reported the well depths for the Gay-Berne potential compared to organic molecules, and they found *e.g.* that well depths $e_{ap} = 6.30, e_{bp} = 1.16, e_{cp} = 0.35$ are a good approximation of sexithiophene. This suggests that well depth ratio $\kappa' = 5$ may be a good approximation for some applications.

4.2 Two-phase system

A two-phase system was created as a starting point for all other simulations. The simulation box size was varied depending on the application and nanoparticle size. A typical case is shown in figure 4.2a, which shows a snapshot of the simulation box of size $(x, y, z) = (68.4\sigma_0, 34.2\sigma_0, 34.2\sigma_0)$ with 32000 fluid particles. The density profile of fluid particles along the x-axis is shown in figure 4.2b. The temperature was set to $T^* = 0.7$, the mean phase densities were calculated to be $\rho_l^* = 0.811 \pm 1.887 \times 10^{-6}$

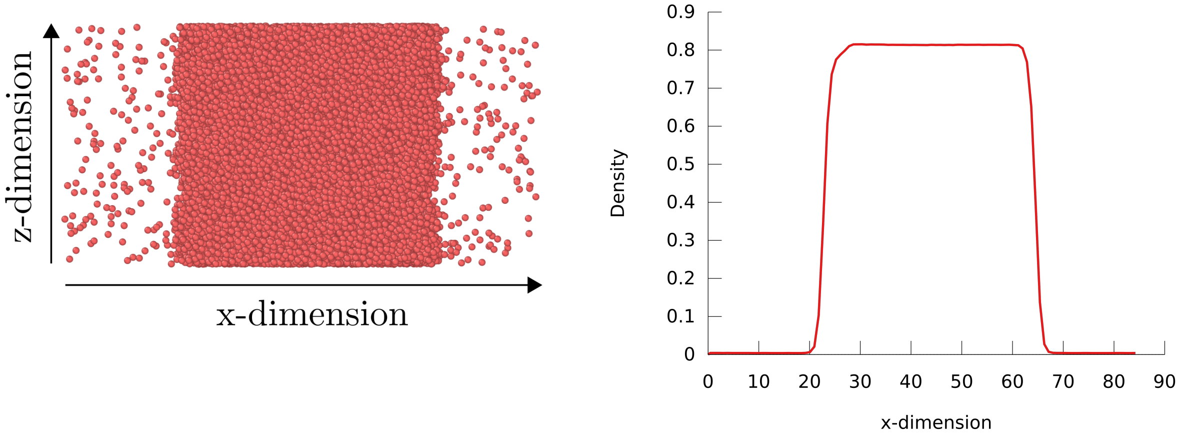

(a) **(b)**

Figure 4.2: **(a)** Snapshot of the simulation box after equilibration. The fluid particles are shown in red. **(b)** Density profile of the two-phase system after equilibration along the x-axis.

and $\rho_v^* = 0.003 \pm 1.4725 \times 10^{-6}$, and the interface thickness was calculated to be $w = 1.189 \pm 5.779 \times 10^{-4}\sigma_0$. The liquid-vapour interface tension was calculated to be $\gamma_{lv}^* = 0.883 \pm 8.213 \times 10^{-3}$.

4.3 Wetting properties

The wetting of a nanoparticle describes the equilibrium position of the nanoparticle in relation to the liquid-vapour interface. A highly wetting nanoparticle will submerge in the liquid phase, a non-wetting nanoparticle will submerge in the vapour phase and a partially wetting nanoparticle will adsorb at the liquid-vapour interface. A nanoparticle was placed at the liquid-vapour interface of a two-phase system, as seen in figure 4.3a. The figure shows a snapshot top-down of a nanoparticle of radii $a = 7.5\sigma_0, b = c = 2.5\sigma_0$ adsorbed at a liquid-vapour interface. The mean distance between the nanoparticle centre of mass and the liquid-vapour interface, $\langle l \rangle$, was calculated as a function of the well depth of the fluid-nanoparticle interaction, ϵ_{fp}. Figure 4.3b shows the wetting of the nanoparticle during equilibration. The nanoparticle was found to equilibrate quickly on the interface. The wetting, l, is normalised by the short radius of the nanoparticle, b. This implies that a wetting $\frac{l}{b} > 1$ corresponds to a nanoparticle that is completely in the liquid side of the Gibbs dividing surface, while a wetting $\frac{l}{b} < -1$ corresponds to a nanoparticle that is completely in the gas side of the Gibbs dividing surface. This is correct if the

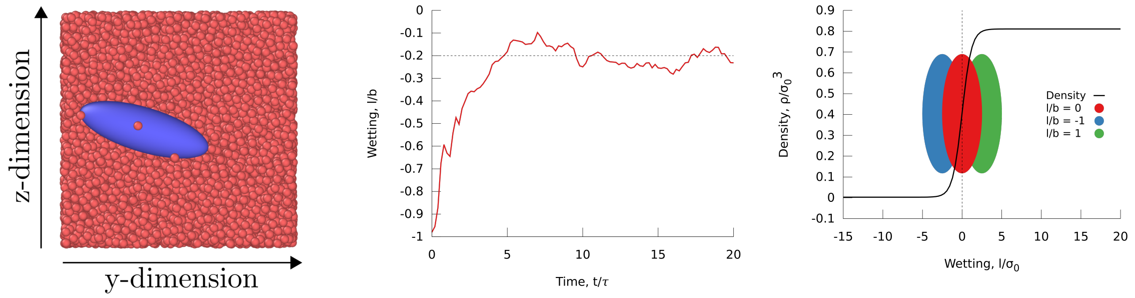

(a) **(b)** **(c)**

Figure 4.3: **(a)** A top-down snapshot of a nanoparticle of radii $a = 7.5\sigma_0, b = c = 2.5\sigma_0$ adsorbed at a liquid-vapour interface. **(b)** The wetting of a nanoparticle of size $a = 7.5\sigma_0, b = c = 2.5\sigma_0$ during equilibration. **(c)** The density profile of the liquid-vapour interface, and three nanoparticles of radii $a = 7.5\sigma_0, b = c = 2.5\sigma_0$ with wettabilities $\frac{l}{b} = 0$ (red), $\frac{l}{b} = -1$ (blue), and $\frac{l}{b} = 1$ (green). The dotted line represents Gibbs dividing surface.

nanoparticles is assumed to be laying flat, with the long axis of the nanoparticle parallel to the Gibbs dividing surface. However, the interface between the liquid-vapour is not a discrete change, but rather a continuous change. This implies that a nanoparticle with wetting $\frac{l}{b} > 1$ still is affected by the interface. Figure 4.3c shows three nanoparticles of radii $a = 7.5\sigma_0, b = c = 2.5\sigma_0$ and wettabilities $\frac{l}{b} = -1$, $\frac{l}{b} = 0$ and $\frac{l}{b} = -1$ in relation to the density profile of the interface. The nanoparticle size is correct in relation to the x-axis. The densities of the fluid at the different positions of the nanoparticles are $\rho^*(-2.5) = 0.015$, $\rho^*(0) = 0.407$ and $\rho^*(2.5) = 0.799$. This illustrates that nanoparticles of a wide range of wettabilities still is attached to the liquid-vapour interface.

The mean wetting, $\langle\frac{l}{b}\rangle$, of nanoparticles of radii $a = 7.5\sigma_0, b = c = 2.5\sigma_0$, $a = 5.0\sigma_0, b = c = 2.5\sigma_0$, $a = 4.5\sigma_0, b = c = 1.5\sigma_0$ and $a = 1.5\sigma_0, b = c = 0.5\sigma_0$ and well depth ratio $\kappa' = 5$ as a function of well depth ϵ_{fp} was calculated, and is shown in figure 4.4. The error bars are given as the standard deviation of the mean, $\sigma_{\langle l/b\rangle}$. The statistical inefficiency for the wetting $\frac{l}{b}$ was calculated to be $s \approx 4000$, implying that the wetting $\frac{l}{b}$ was calculated every 4000 timestep. The wetting as a function of the well depth is close to linear for $|\frac{l}{b}| < 1$, and a linear regression of this region was computed. This regression was used to calculate the well depth corresponding to the wetting wanted in later computations. For the nanoparticle of radii $a = 5.0\sigma_0, b = c = 2.5\sigma_0$ in the region $10\epsilon_0 < \epsilon_{fp} < 12\epsilon_0$, the wetting changes dramatically. This region corresponds to wetting $0.5\sigma_0 < \frac{l}{b} < 1.5\sigma_0$. For these wettabilities it is later shown that the nanoparticle prefer a

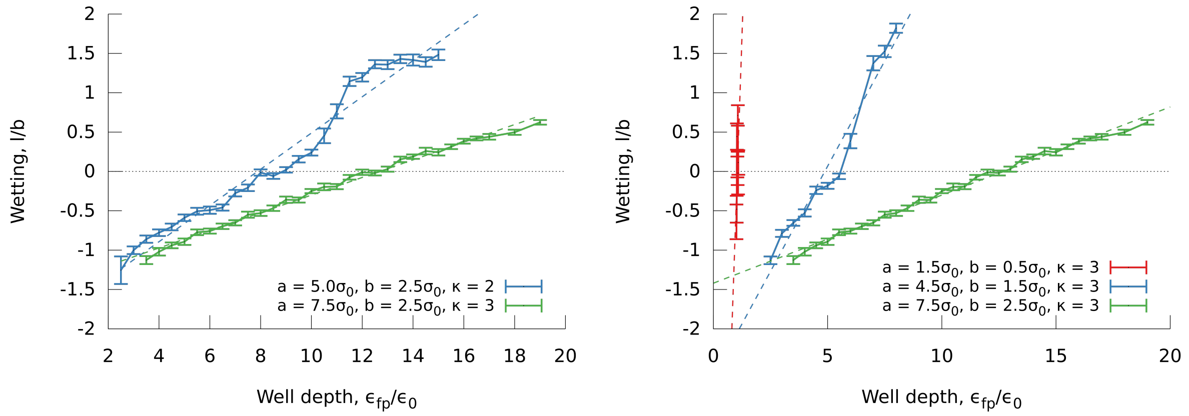

(a) **(b)**

Figure 4.4: Nanoparticles of well depth ratio $\kappa' = 5$. The mean wetting $\langle \frac{l}{b} \rangle$ of nanoparticles of radii $a = 7.5\sigma_0, b = c = 2.5\sigma_0$, $a = 5.0\sigma_0, b = c = 2.5\sigma_0$, $a = 4.5\sigma_0, b = c = 1.5\sigma_0$ and $a = 1.5\sigma_0, b = c = 0.5\sigma_0$ as a function of well depth ϵ_{fp}.

pitch close to $\phi = 0$ or $\phi = \frac{\pi}{2}$.

The mean wetting, $\langle \frac{l}{b} \rangle$, of nanoparticles of radii $a = 7.5\sigma_0, b = c = 2.5\sigma_0$, $a = 5.0\sigma_0, b = c = 2.5\sigma_0$, $a = b = c = 2.5\sigma_0$, $a = 4.5\sigma_0, b = c = 1.5\sigma_0$ and $a = 1.5\sigma_0, b = c = 0.5\sigma_0$, and well depth ratio $\kappa' = 1$ as a function of well depth, ϵ_{fp}, was calculated, and is presented in figure 4.5. The well depth of the nanoparticles with well depth ratio $\kappa' = 5$ is generally higher compared to the nanoparticles with well depth ratio $\kappa' = 1$ for the same wetting $\frac{l}{b}$. This is because the well depth on the tips of the nanoparticles with well depth ratio $\kappa' = 5$ is much lower than the sides, and the well depth on the sides needs to compensate. The nanoparticles of radii $a = 1.5\sigma_0, b = c = 0.5\sigma_0$ were unstable at the liquid-vapour interface, and it was difficult to obtain a wetting close to $|\frac{l}{b}| \approx 1$.

4.3.1 Pitch

The pitch, ϕ, of a nanoparticle adsorbed at a liquid-vapour interface was calculated. The pitch is the angle between a vector normal to the interface and a vector parallel to the long axis of the nanoparticle. It is calculated as $\cos\phi = \boldsymbol{e}_i \cdot \boldsymbol{x}$, where $\boldsymbol{e}_i$ is a unit vector parallel to the long axis of the nanoparticle and $\boldsymbol{x} = [1, 0, 0]$, which is normal to the liquid-vapour interface. Pitch $\phi = \frac{\pi}{2}$ corresponds to a nanoparticle laying flat on the interface with the long axis parallel to the interface, and pitches $\phi = 0$ and $\phi = \pi$ correspond to the

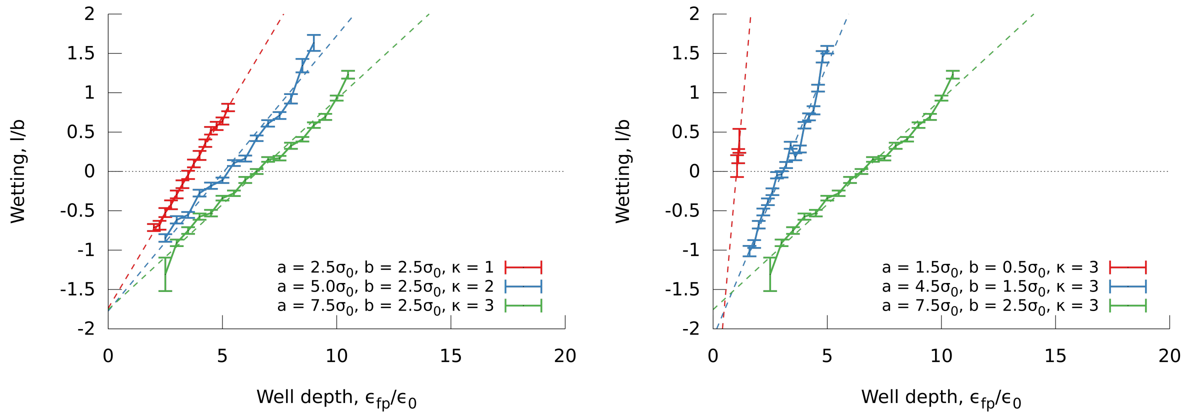

(a) **(b)**

Figure 4.5: Nanoparticles of well depth ratio $\kappa' = 1$. The mean wetting $\langle \frac{l}{b} \rangle$ of nanoparticles of radii $a = 7.5\sigma_0, b = c = 2.5\sigma_0$, $a = 5.0\sigma_0, b = c = 2.5\sigma_0$, $a = b = c = 2.5\sigma_0$, $a = 4.5\sigma_0, b = c = 1.5\sigma_0$ and $a = 1.5\sigma_0, b = c = 0.5\sigma_0$ as a function of well depth ϵ_{fp}.

long axis of the nanoparticle perpendicular to the interface. Pitches $\phi = 0$ and $\phi = \pi$ are equivalent, as the prolate ellipsoidal nanoparticles are symmetrical. The pitch ranges from 0 to π, which implies that a nanoparticle where all pitches are equally likely will have a mean pitch $\langle \phi \rangle = \frac{\pi}{2}$. These particles may be distinguished from nanoparticles that are adsorbed at the interface with a mean pitch $\langle \phi \rangle = \frac{\pi}{2}$ by inspecting the standard deviation of the pitch, as this will be much higher for nanoparticles where all pitches are equally likely.

The mean pitch, $\langle \phi \rangle$, as a function of the mean wetting, $\langle \frac{l}{b} \rangle$, for for nanoparticles of radii $a = 7.5\sigma_0, b = c = 2.5\sigma_0$ and well depth ratios $\kappa' = 5$ and $\kappa' = 1$ is presented in figure 4.6. The error bars are given as the standard deviation σ_ϕ. The nanoparticles with a mean wetting $|\frac{l}{b}| < 1$ have a mean pitch $\phi \approx \frac{\pi}{2}$ and a low standard deviation, which suggest that the pitch is reasonably stable. This is as expected, because the pitch $\phi = \frac{\pi}{2}$ corresponds to the lowest free energy of a prolate ellipsoidal nanoparticle adsorbed at a liquid-vapour interface. Nanoparticles in the region $|\frac{l}{b}| > 1$ have higher standard deviation. This suggests that the pitch varies more, and that these particles are not as stable as the particles more closely adsorbed at the liquid-vapour interface. In the region $1 < \frac{l}{b} < 2$, for nanoparticles with well depth ratio $\kappa' = 5$, the pitches were $\phi \approx \frac{\pi}{4}$ and $\phi \approx \frac{3\pi}{4}$, which are equivalent. This is not the case for nanoparticles with well depth ratio $\kappa' = 1$, which suggests that a nanoparticle with wettability $1 < \frac{l}{b} < 2$ and well depth ratio $\kappa' = 5$,

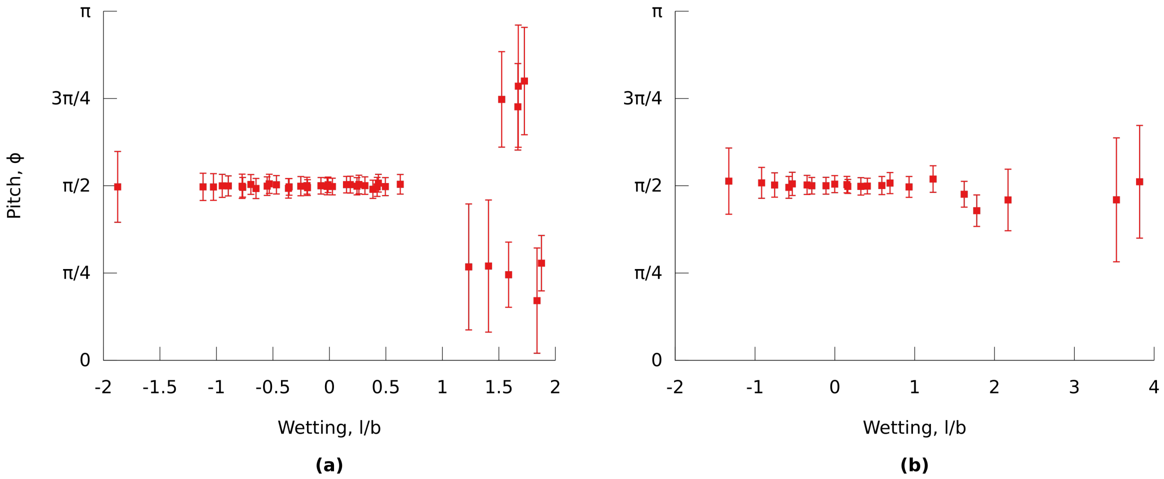

Figure 4.6: The mean pitch, $\langle\phi\rangle$, as a function of wetting, $\frac{l}{b}$, for a nanoparticle of size $a = 7.5\sigma_0, b = c = 2.5\sigma_0$. Nanoparticles with well depth ratio **(a)** $\kappa' = 5$ and **(b)** $\kappa' = 1$.

prefers to be oriented with the tip of the nanoparticle out in the vapour phase. This is because the interaction between the fluid and the nanoparticle tip is weaker than the interaction with the side of the nanoparticle. This results in the fluid to attract strongly to the side, while avoiding the tip. The pitches $\phi = 0$ and $\phi = \frac{\pi}{2}$ give the largest area of contact between fluid and nanoparticle side, and smallest area of contact between fluid and nanoparticle tip, because one tip will stick out in the vapour phase. There was a distinct difference between the state observed for wetting $|\frac{l}{b}| < 1$ and the state observed for wetting $1 < \frac{l}{b} < 2$. It is clear that a certain degree of wetting is needed to obtain this preferred orientation. Presumably, a higher degree of wetting will cause the nanoparticle tip to be adequately attracted to the fluid, which will cause the nanoparticle to completely submerge in the bulk liquid.

The mean pitch, $\langle\phi\rangle$, as a function of the mean wetting, $\langle\frac{l}{b}\rangle$, for nanoparticles of radii $a = 5.0\sigma_0, b = c = 2.5\sigma_0$, and well depth ratios $\kappa' = 5$ and $\kappa' = 1$ is presented in figure 4.7. In the region $-1 < \frac{l}{b} < -0.5$, the nanoparticles were closely adsorbed at the liquid-vapour interface, and the pitch was $\phi = \frac{\pi}{2}$. This is similar to nanoparticles of radii $a = 7.5\sigma_0, b = c = 2.5\sigma_0$. However, the standard deviation is higher. This suggests that nanoparticles with a shorter long axis a have less stable pitches. This is reasonable, as shorter nanoparticles requires less energy to rotate compared to longer nanoparticles. Nanoparticles of wetting $\frac{l}{b} < -2.5$ with well depth ratio $\kappa' = 5$ and nanoparticles of

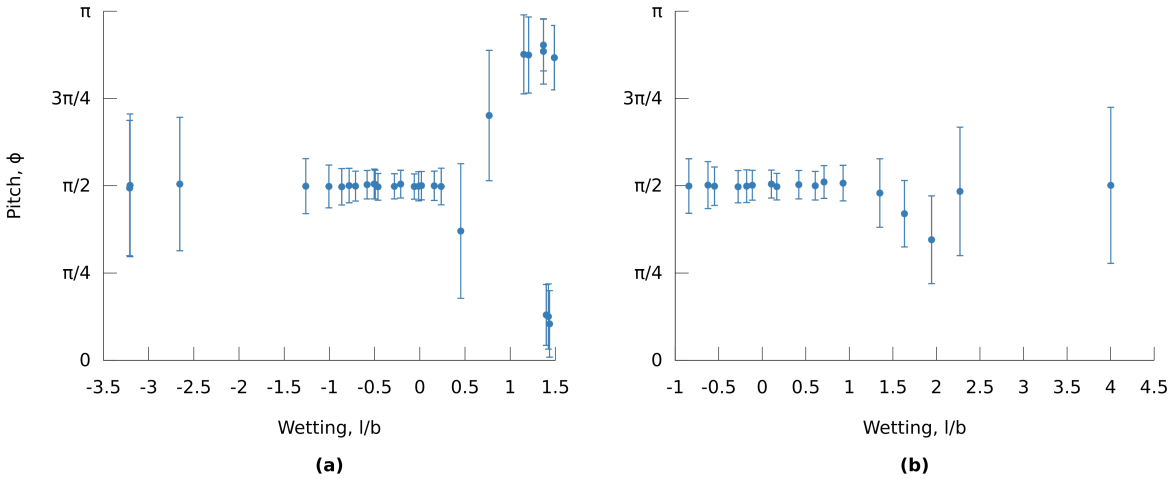

Figure 4.7: The mean pitch, $\langle\phi\rangle$, as a function of wetting, $\frac{l}{b}$, for a nanoparticle of size $a = 5.0\sigma_0, b = c = 2.5\sigma_0$. Nanoparticles with well depth ratio **(a)** $\kappa' = 5$ and **(b)** $\kappa' = 1$.

wetting $\frac{l}{b} < 2$ with well depth ratio $\kappa' = 1$ have high standard deviations, and it is reasonable to conclude that the pitches of these nanoparticles are fairly unstable. This implies that their rotation is less affected by the interface. In the region $1 < \frac{l}{b} < 1.5$, for nanoparticles with well depth ratio $\kappa' = 5$, the same phenomena as discussed above is observed, the nanoparticles prefer pitches $\phi \approx 0$ or $\phi \approx \frac{\pi}{2}$. The standard deviations of these particles are lower compared to the nanoparticles of radii $a = 7.5\sigma_0, b = c = 2.5\sigma_0$, and they are closer to pitches $\phi \approx 0$ or $\phi \approx \frac{\pi}{2}$. This may be explained by the long radii a being shorter, implying that less energy is needed to rotate the nanoparticle from a pitch $\phi = \frac{\pi}{2}$ to pitch $\phi = 0$ or $\phi = \pi$.

The mean pitch, $\langle\phi\rangle$, as a function of the mean wetting, $\langle\frac{l}{b}\rangle$, is presented in figure 4.8 and 4.9 for nanoparticles of radii $a = 4.5\sigma_0, b = c = 1.5\sigma_0$ and $a = 1.5\sigma_0, b = c = 0.5\sigma_0$, respectively. Both figures present nanoparticles with well depth ratios $\kappa' = 5$ and $\kappa' = 1$. Nanoparticles of radii $a = 4.5\sigma_0, b = c = 1.5\sigma_0$ exhibit the same phenomena as described for nanoparticles of radii $a = 7.5\sigma_0, b = c = 2.5\sigma_0$ and $a = 5.0\sigma_0, b = c = 2.5\sigma_0$. Nanoparticles of radii $a = 1.5\sigma_0, b = c = 0.5\sigma_0$ have a high standard deviation for all wettabilities, and the mean pitch is $\phi \approx \frac{\pi}{2}$. This suggests that the pitch of the nanoparticle is unstable. This nanoparticle is too small, and the energy needed to rotate the nanoparticle is too small for it to be stable at the interface.

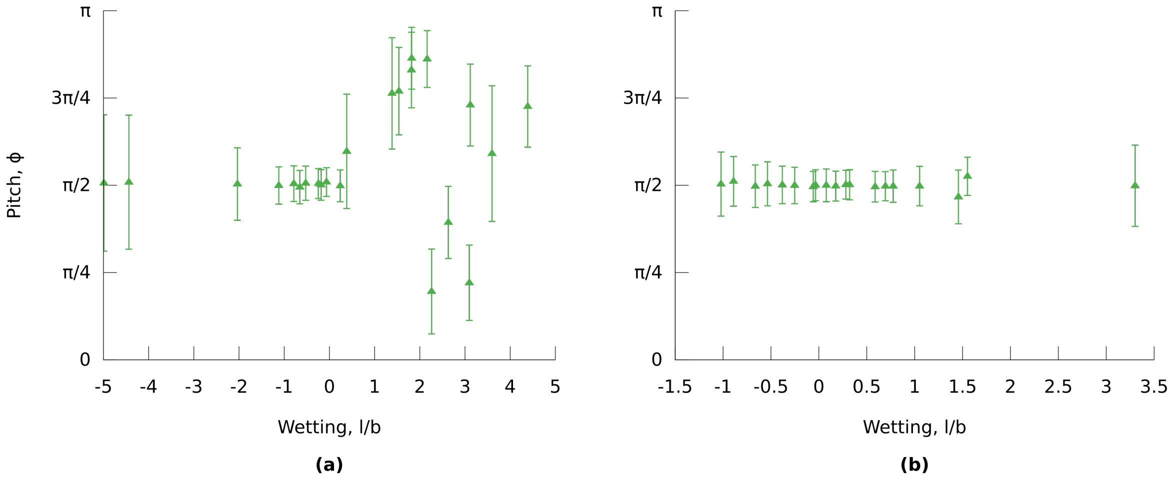

Figure 4.8: The mean pitch, $\langle\phi\rangle$, as a function of wetting, $\frac{l}{b}$, for a nanoparticle of size $a = 4.5\sigma_0, b = c = 1.5\sigma_0$. Nanoparticles with well depth ratio **(a)** $\kappa' = 5$ and **(b)** $\kappa' = 1$.

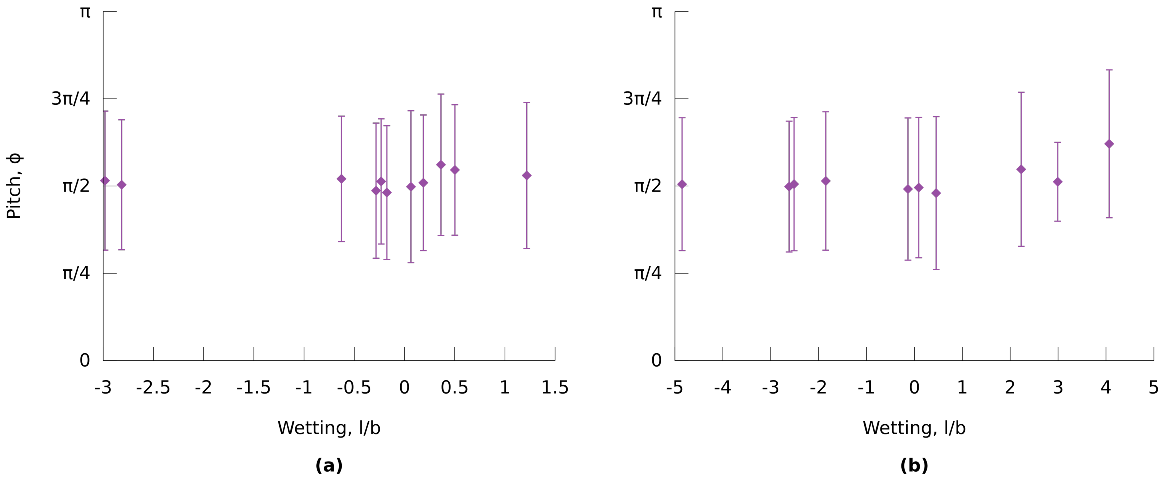

Figure 4.9: The mean pitch, $\langle\phi\rangle$, as a function of wetting, $\frac{l}{b}$, for a nanoparticle of size $a = 1.5\sigma_0, b = c = 0.5\sigma_0$. Nanoparticles with well depth ratio **(a)** $\kappa' = 5$ and **(b)** $\kappa' = 1$.

4.4 Brownian motion

The Brownian motion and self-diffusion were calculated for nanoparticles adsorbed at a liquid-vapour interface. The self-diffusion determines the collision rates of nanoparticles. If the self-diffusion is very low, and there are few nanoparticles, they will never interact. A nanoparticle was placed at the liquid-vapour interface of a two-phase system. The nanoparticle was then equilibrated at the interface, and the movement and mean-square displacement of a single nanoparticle adsorbed at a liquid-vapour interface was calculated. The mean-square displacement was calculated as described in section 2.2.2. Figures 4.10 and 4.11 show the movement of nanoparticles projected down on the yz-plane, which is parallel to the liquid-vapour interface plane. The marker shows the position of the nanoparticle at different timesteps and the dotted line shows the path of the nanoparticle. For the prolate ellipsoidal nanoparticles (figure 4.10 and 4.11) the arrow shows the orientation of the nanoparticle, where the arrow is parallel to the long axis of the nanoparticle. The markers are equally spaced in time, implying that the marker-marker distance may be considered as the velocity of the nanoparticle. The colour of the marker represents the wetting of the nanoparticle at the different timesteps. Blue corresponds to a wetting $\frac{l}{b} > -1$, a nanoparticle that is completely in the gas side of the interface. Red corresponds to a wetting $-1 < \frac{l}{b} < 1$, a nanoparticle tightly adsorbed at the liquid-vapour interface. Green corresponds to a wetting $\frac{l}{b} < 1$, a nanoparticle that is completely in the liquid side of the interface. However, the interface between the liquid-vapour is not a discrete change in density, but rather a continuous change. This means that for a wetting $\frac{l}{b} \approx -1$ for $b = 2.5\sigma_0$, the nanoparticle will still be affected by the interface.

Figure 4.10a shows the movement of a prolate ellipsoidal nanoparticle of radii $a = 7.5\sigma_0, b = c = 2.5\sigma_0$ and mean wetting $\langle \frac{l}{b} \rangle = -0.02 \pm 1.50 \times 10^{-3}$. The nanoparticle seems to prefer moving along to the long axis of the nanoparticle. This is reasonable, as movement in that direction has the least amount of resistance. The nanoparticle orientation over time suggests that the rotation is moderately restricted, as the nanoparticle never does a full revolution. Figure 4.10b shows the movement of a spherical nanoparticle of radii $a = b = c = 2.5\sigma_0$ and mean wetting $\langle \frac{l}{b} \rangle = -0.05 \pm 2.17 \times 10^{-3}$. These results show that the nanoparticles of these sizes may be stable at the liquid-vapour interface, as it never moves out of the region $|\frac{l}{b}| < 1$ for a simulation of length of approximately 20 ns.

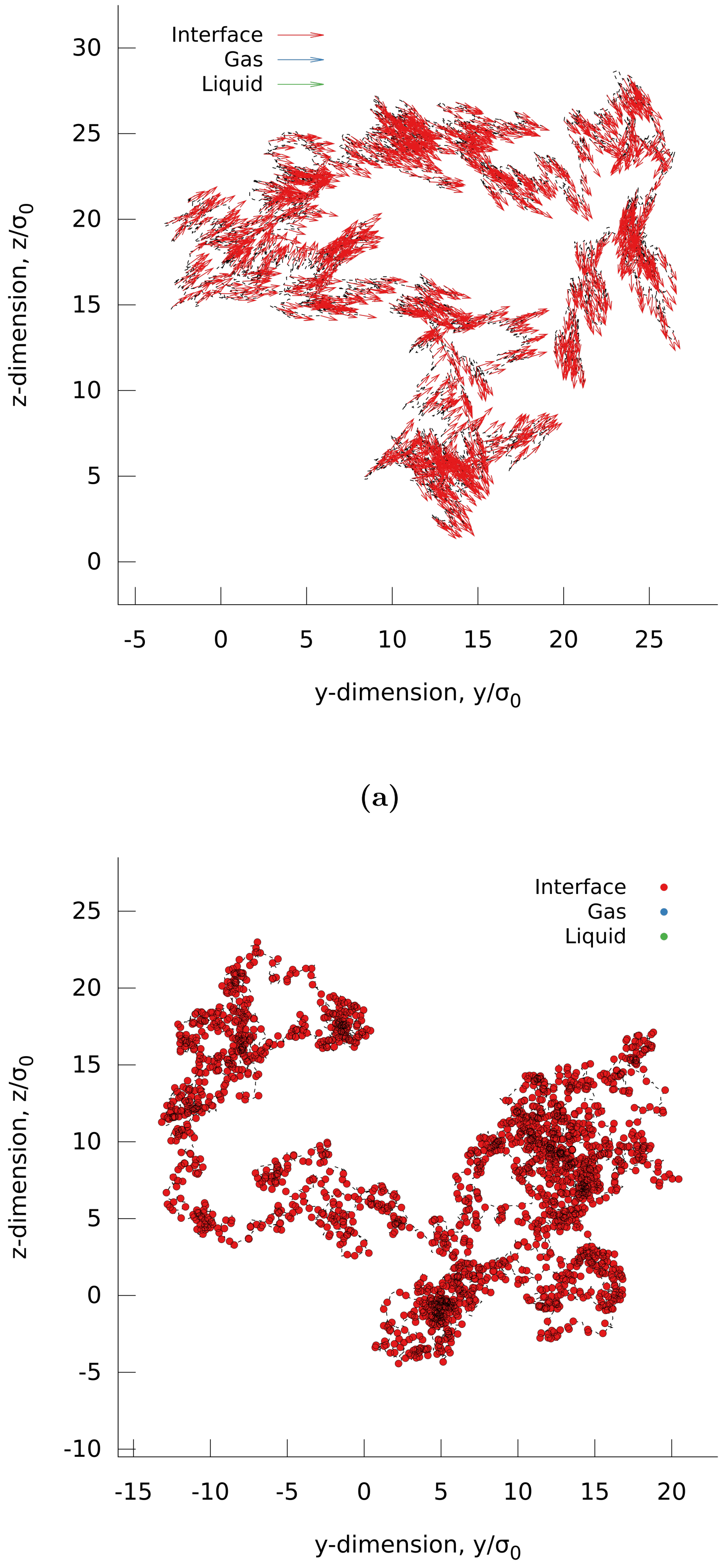

(a)

(b)

Figure 4.10: The Brownian motion of **(a)** a prolate ellipsoidal nanoparticle of radii $a = 7.5\sigma_0, b = c = 2.5\sigma_0$ and wetting $\langle \frac{l}{b} \rangle = -0.02 \pm 1.50 \times 10^{-3}$, and **(b)** a spherical nanoparticle of radii $a = b = c = 2.5\sigma_0$ and wetting $\langle \frac{l}{b} \rangle = -0.05 \pm 2.17 \times 10^{-3}$.

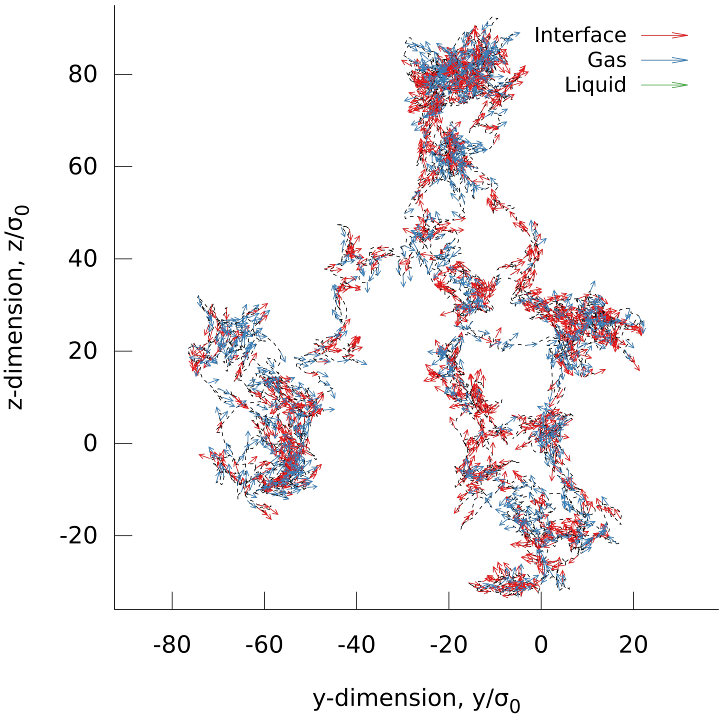

(a)

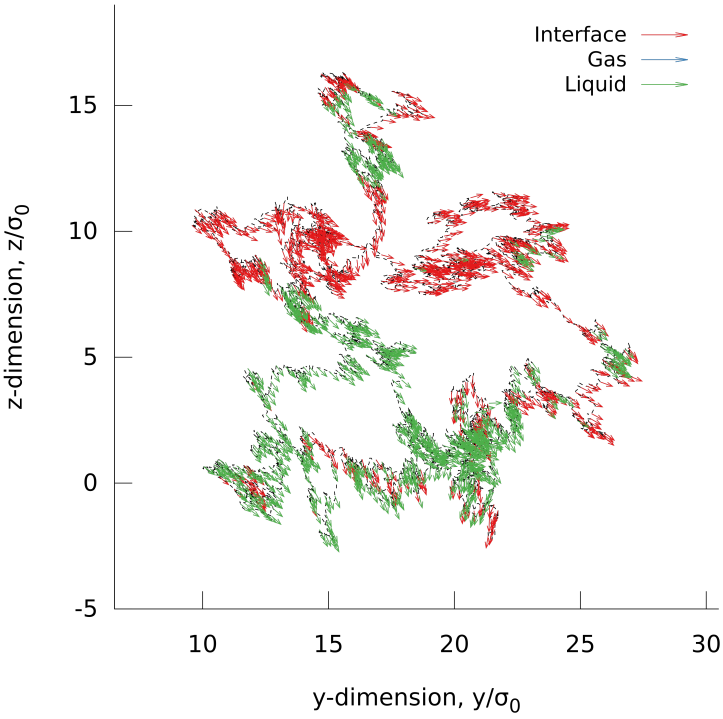

(b)

Figure 4.11: The Brownian motion of **(a)** a prolate ellipsoidal nanoparticle of radii $a = 7.5\sigma_0, b = c = 2.5\sigma_0$ and wetting $\langle \frac{l}{b} \rangle = -0.98 \pm 2.26 \times 10^{-3}$, and **(b)** a prolate ellipsoidal nanoparticle of radii $a = 7.5\sigma_0, b = c = 2.5\sigma_0$ and wetting $\langle \frac{l}{b} \rangle = 1.04 \pm 3.19 \times 10^{-3}$.

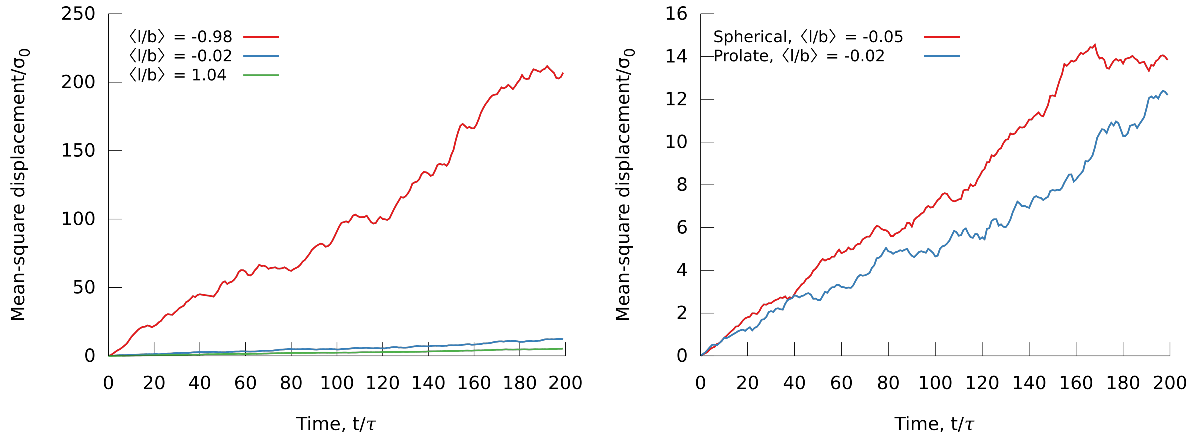

(a) **(b)**

Figure 4.12: Mean-square displacement of nanoparticles adsorbed at the liquid-vapour interface. **(a)** Nanoparticles of radii $a = 7.5\sigma_0, b = c = 2.5\sigma_0$ and wettabilities $\langle \frac{l}{b} \rangle = -0.98 \pm 2.26 \times 10^{-3}$ in red, $\langle \frac{l}{b} \rangle = 0.02 \pm 1.50 \times 10^{-3}$ in blue, and $\langle \frac{l}{b} \rangle = 1.04 \pm 3.19 \times 10^{-3}$ in green. **(b)** Nanoparticles of radii $a = 7.5\sigma_0, b = c = 2.5\sigma_0$ and $a = b = c = 2.5\sigma_0$ with wettabilities $\langle \frac{l}{b} \rangle = 0.02 \pm 1.50 \times 10^{-3}$ and $\langle \frac{l}{b} \rangle = 0.05 \pm 2.17 \times 10^{-3}$, respectively.

Figure 4.11a shows the movement of a nanoparticle of radii $a = 7.5\sigma_0, b = c = 2.5\sigma_0$ with mean wetting $\langle \frac{l}{b} \rangle = -0.98 \pm 2.26 \times 10^{-3}$. The figure shows that the nanoparticle may detach from the interface, and then reattach at a later time point. During these events the nanoparticle is able to move with a higher velocity, compared to when it is attached to the liquid-vapour interface. During the events of detachment, the nanoparticle moves both side to side and backwards and forwards. This may be due to a low vapour phase density, which makes the orientation of the nanoparticles less significant. The nanoparticle orientation changes more freely in this wettability, compared to the nanoparticle in figure 4.10a. This is caused by the density difference of the liquid-vapour interface. Figure 4.11b shows the movement of a nanoparticle of radii $a = 7.5\sigma_0, b = c = 2.5\sigma_0$ with mean wetting $\langle \frac{l}{b} \rangle = 1.04 \pm 3.19 \times 10^{-3}$. This figure shows the same characteristics as for the nanoparticle with wetting $\langle \frac{l}{b} \rangle = -0.02$, seen in figure 4.10a, and shows that the orientation of nanoparticles with this wettability is greatly restricted.

Figure 4.12 shows the mean-square displacement of nanoparticles adsorbed at the liquid-vapour interface with varying wettabilities and nanoparticle sizes. The mean-square displacement was only calculated in the yz-plane, which is parallel to the liquid-vapour interface. The simulation was run for a time $t^* = 10000$, and was split into 50 blocks. The mean-square displacement was averaged over all the blocks. Figure 4.12a shows the mean-square displacement of nanoparticles of radii $a = 7.5\sigma_0, b = c = 2.5\sigma_0$ and wettabilities $\langle \frac{l}{b} \rangle = -0.98 \pm 2.26 \times 10^{-3}$, $\langle \frac{l}{b} \rangle = -0.02 \pm 1.50 \times 10^{-3}$ and $\langle \frac{l}{b} \rangle = 1.04 \pm 3.19 \times 10^{-3}$. The self-diffusion was much greater for a nanoparticle with a low wettability, compared to a partially or fully wetting nanoparticle. This is caused by the density of the vapour phase, which is much lower than the density of the liquid phase. If the two-phase system was of two immiscible liquids with equal densities, this would not be the case. The self-diffusion does not change as dramatically from a wetting $\frac{l}{b} \approx 0$ to $\frac{l}{b} \approx 1$, as it does from $\frac{l}{b} \approx -1$ to $\frac{l}{b} \approx 0$. Figure 4.12b shows the mean-square displacement of nanoparticles of radii $a = 7.5\sigma_0, b = c = 2.5\sigma_0$ and $a = b = c = 2.5\sigma_0$ and wettabilities $\langle \frac{l}{b} \rangle = 0.02 \pm 1.50 \times 10^{-3}$ and $\langle \frac{l}{b} \rangle = 0.05 \pm 2.17 \times 10^{-3}$, respectively. This shows that the mean-square displacement of a prolate ellipsoidal nanoparticle adsorbed at a liquid-vapour interface is roughly equal the mean-square displacement of a spherical nanoparticle adsorbed at a liquid-vapour interface, even though the surface area of the prolate ellipsoid nanoparticle is approximately 2.5 greater than the spherical nanoparticle. This may be because the prolate ellipsoidal nanoparticle primarily moves in the direction parallel to the long axis of the nanoparticle, which has the same radii as the spherical nanoparticle.

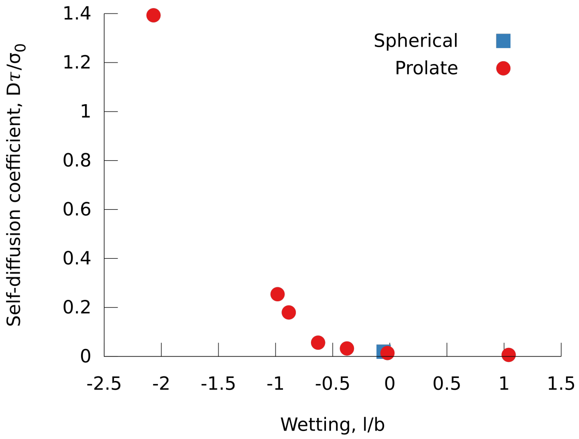

Figure 4.13: The two-dimensional self-diffusion coefficient, D, as a function of wetting, $\frac{l}{b}$, for nanoparticles of radii $a = 7.5\sigma_0, b = c = 2.5\sigma_0$ (red circle) and $a = b = c = 2.5\sigma_0$ (blue square).

The two-dimensional self-diffusion coefficients was calculated, with equation 2.14, and is plotted as a function of the mean wetting in figure 4.13. The two-dimensional self-diffusion coefficient quantify the velocity of Brownian motion along the liquid-vapour interface. The results show a clear change in the self-diffusion coefficient between $\frac{l}{b} = -1.0$ and $\frac{l}{b} = 0.0$. As the wetting decreases, and the nanoparticle gets completely detached

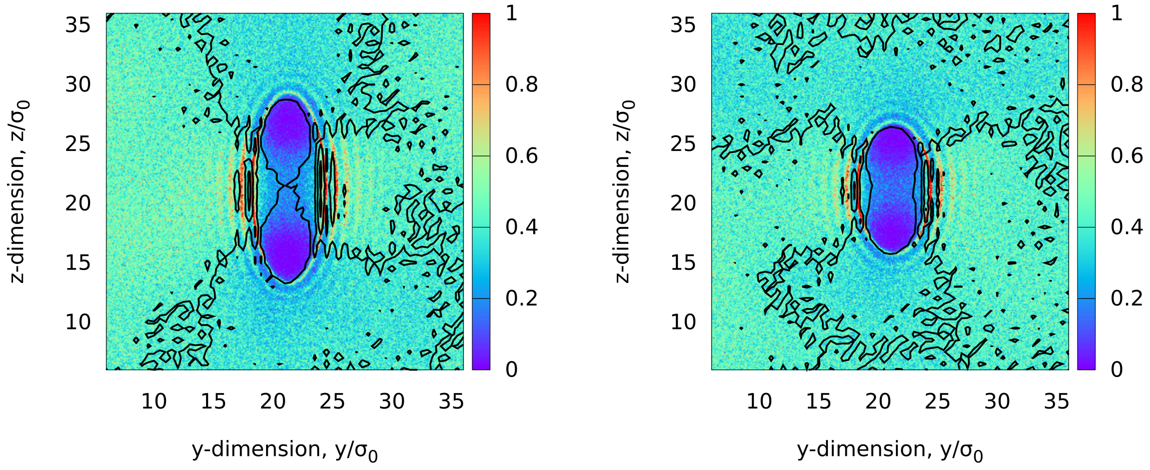

(a) **(b)**

Figure 4.14: Local density of fluid particles in a slab of thickness equal to the short diameter of the nanoparticle, $2b = 5.0\sigma_0$, around the nanoparticle adsorbed at a liquid-vapour interface. The nanoparticles are of well depth ratio $\kappa' = 5$ and **(a)** radii $a = 7.5\sigma_0, b = c = 2.5\sigma_0$ and wetting $l/b = 0.628$, and **(b)** radii $a = 5.0\sigma_0, b = c = 2.5\sigma_0$ and wetting $l/b = 0.676$.

from the interface, the self-diffusion coefficient as a function of the wetting will most likely flatten and become constant.

4.5 Interface deformation

Prolate ellipsoidal nanoparticles are predicted to induce static fluid interface deformations [7]. In order to investigate this, a prolate ellipsoidal nanoparticle was placed at the liquid-vapour interface of a two-phase system and the local density of fluid particles around it was calculated. A slab of fluid particles of thickness $2b = 5.0\sigma_0$ was considered. The slab was centred on the nanoparticle centre off mass, which had a mean wetting $l/b \approx 0.71$. This corresponds to a contact angle $\theta = 45°$. The slab was divided into bins with side length $0.1\sigma_0$.

Figure 4.14a and 4.14b show a top-down view of the local fluid particle density around the nanoparticles of size $a = 7.5\sigma_0, b = c = 2.5\sigma_0$ and $a = 5.0\sigma_0, b = c = 2.5\sigma_0$, respectively, adsorbed at a liquid-vapour interface with well depth ratio $\kappa' = 5$. The colour represents the local fluid density. Bright red represents density $\rho^* = 1$ and dark

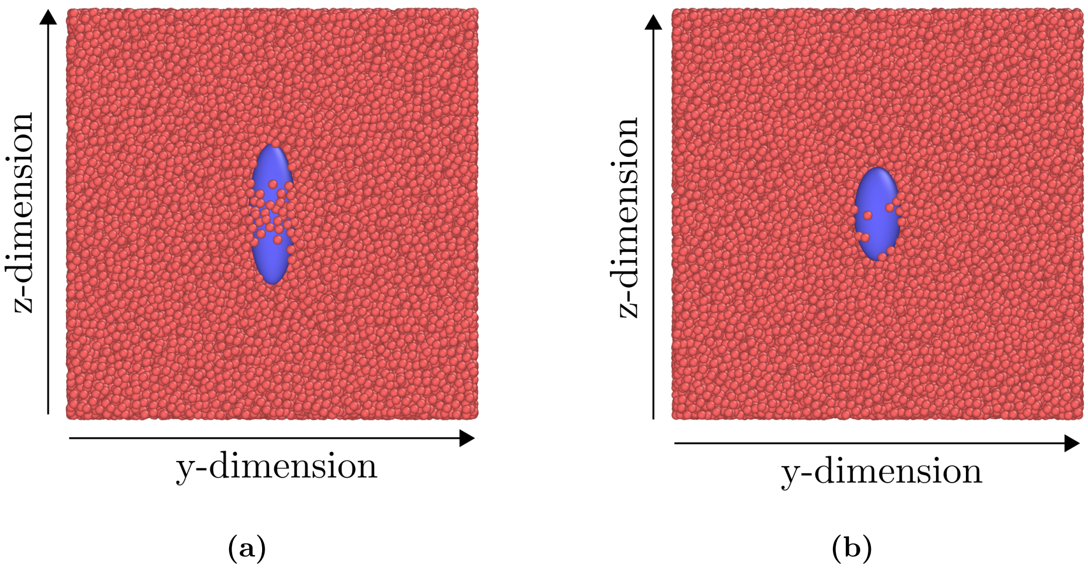

(a) **(b)**

Figure 4.15: Snapshot of nanoparticles of well depth ratio $\kappa' = 5$ and radii **(a)** $a = 7.5\sigma_0, b = c = 2.5\sigma_0$ and **(b)** $a = 5.0\sigma_0, b = c = 2.5\sigma_0$ adsorbed at a liquid-vapour interface. The fluid particles in red are in a slab around the nanoparticles in blue.

blue represents density $\rho^* = 0$. The black lines are contour lines, and are drawn with an equidistance of $\rho^* = 0.2$. The contour lines are drawn with a lower resolution, and the bins has a side length of $0.5\sigma_0$. There was a higher density of fluid particles around the sides of the nanoparticles compared to the tips. This is as expected, as the well depth on the sides is five times greater than on the tips. There was a high degree of fluid particles packed close to the nanoparticle surface, which created a halo of fluid particles around the sides of the nanoparticle. This may be observed the snapshot in figure 4.15a. This is observed to a less degree for the nanoparticle of radii $a = 5.0\sigma_0, b = c = 2.5\sigma_0$, as seen in figure 4.15b.

Figure 4.16a and 4.16b show a top-down view of the fluid particle density around nanoparticles of size $a = 7.5\sigma_0, b = c = 2.5\sigma_0$ and $a = 5.0\sigma_0, b = c = 2.5\sigma_0$, respectively, adsorbed at a liquid-vapour interface with well depth ratio $\kappa' = 1$. These figures show a high degree of packing around the whole nanoparticle, and not only on the sides. In addition, these figures do not show deformation of the interface due to the particle shape. Lehle *et al.* [7] claim that a nanoparticle with aspect ratio $\kappa = 2$ and contact angle $\theta = 45°$ should give a meniscus height of the interface deformation in the order of $\Delta h = 0.1b = 0.25\sigma_0$. This is not observed in these calculations, probably because the

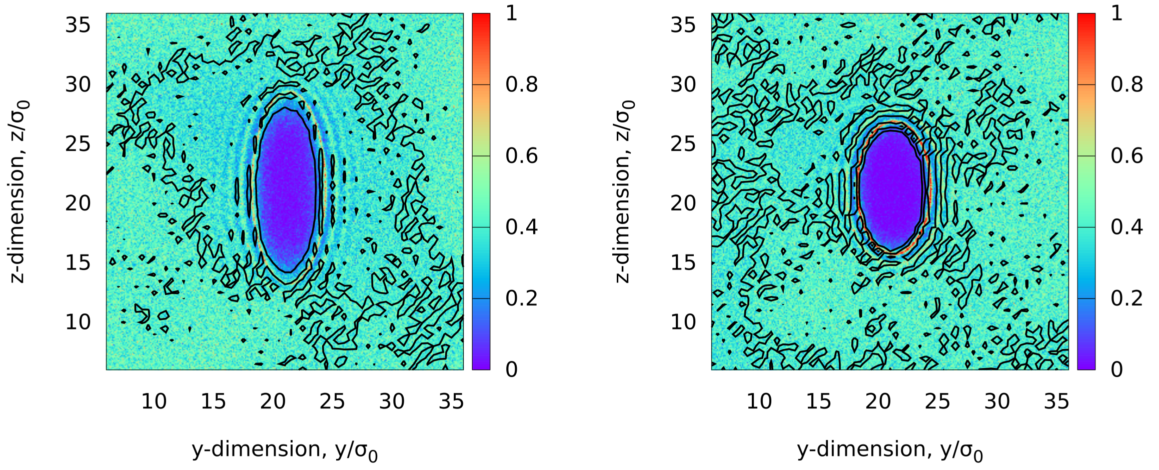

(a) (b)

Figure 4.16: Local density of fluid particles in a slab of thickness equal to the short diameter of the nanoparticle, $2b = 5.0\sigma_0$, around the nanoparticle adsorbed at a liquid-vapour interface. The nanoparticles are of well depth ratio $\kappa' = 1$ and **(a)** radii $a = 7.5\sigma_0, b = c = 2.5\sigma_0$ and wetting $l/b = 0.710$, and **(b)** radii $a = 5.0\sigma_0, b = c = 2.5\sigma_0$ and wetting $l/b = 0.692$.

meniscus height is too small compared to the noise in the calculations. A nanoparticle with the same contact angle and aspect ratio $\kappa = 10$ should give a meniscus height of the interface deformation in the order of $\Delta h \approx 0.4b$. If b is sufficiently large, a deformation due to the shape of the nanoparticle may be observed using this technique. The interface deformation may still be present for nanoparticles of this size, but is too small to observe. The effects of interface deformation, *i.e.* capillary force, may still be present. This can be investigated by calculating the radial distribution function of several of these nanoparticles adsorbed at a liquid-vapour interface.

4.6 Solvent-mediated forces

The solvent-mediated force is the force acting on nanoparticles due to the presence of solvent particles. This was investigated in order to get an understanding of how a large number of these nanoparticle will behave in a two-phase system. The force acting on a nanoparticle-nanoparticle pair with fixed surface-to-surface separation d was calculated as a function of d. The direct nanoparticle-nanoparticle interaction was turned off, and

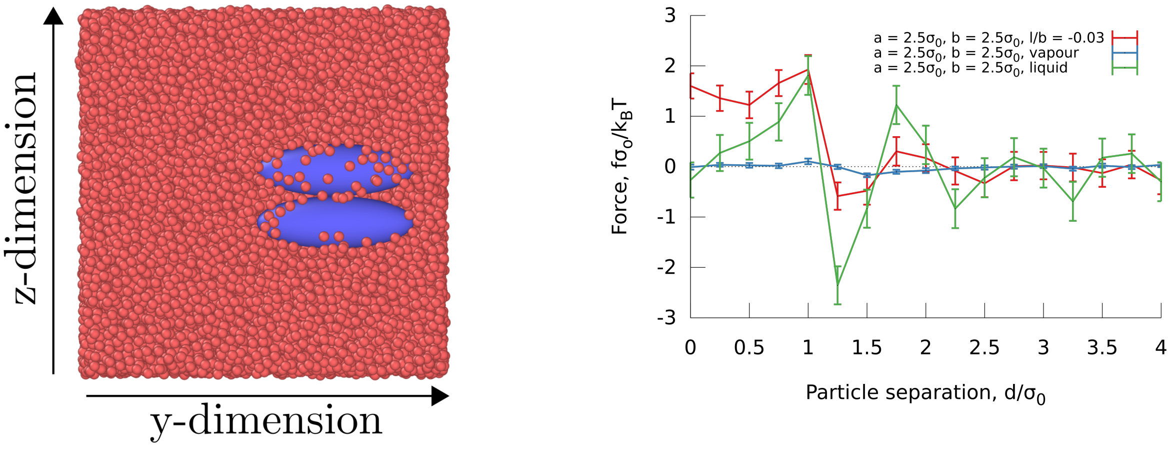

(a) **(b)**

Figure 4.17: **(a)** A top-down snapshot of a nanoparticle-nanoparticle pair of size $a = 7.5\sigma_0, b = c = 2.5\sigma_0$, surface-to-surface separation $d = 0\sigma_0$, and well depth ratio $\kappa' = 1$ adsorbed at a liquid-vapour interface. **(b)** Solvent-mediated force acting on a spherical nanoparticle of radii $a = b = c = 2.5\sigma_0$ and well depth ratio $\kappa' = 1$ as a function of surface-to-surface separation d.

the pair was placed at the liquid-vapour interface and left to equilibrate, as seen in figure 4.17a. The figure shows a nanoparticle-nanoparticle pair of radii $a = 7.5\sigma_0, b = c = 2.5\sigma_0$ and surface-to-surface separation $d = 0$. Cases for nanoparticle pairs submerged in bulk liquid and vapour was also considered. The statistical inefficiency of the force calculations was calculated to be $s \approx 100$, implying that the force was calculated every 100 timestep. The force relates to the potential energy by $f(d) = -\left(\frac{\partial u}{\partial d}\right)$. This implies that whenever the force $f(d) = 0$, there is a local minimum or maximum in the potential energy $u(d)$.

4.6.1 Spherical nanoparticles

The solvent-mediated force acting on spherical nanoparticles of radii $a = b = c = 2.5\sigma_0$, well depth $\epsilon_{fp} = 3.575$, and well depth ratio $\kappa' = 1$ is shown in figure 4.17b. Three different cases were considered: Nanoparticles completely submerged in the gas phase, completely submerged in the liquid phase, and adsorbed at the liquid-vapour interface with mean wetting $\langle \frac{l}{b} \rangle = -0.03 \pm 1.55 \times 10^{-4}$, which corresponds to a contact angle $\theta = 91.7°$. The well depth, ϵ_{fp}, was the same for all three cases, which implies that if the nanoparticles completely submerged in the bulk phases were in range of a liquid-vapour interface, it would adsorb at the interface rather than being submerged in the bulk phases. The force exhibits oscillations that decay with increasing d for $d > \sigma_0$, caused by the packing of

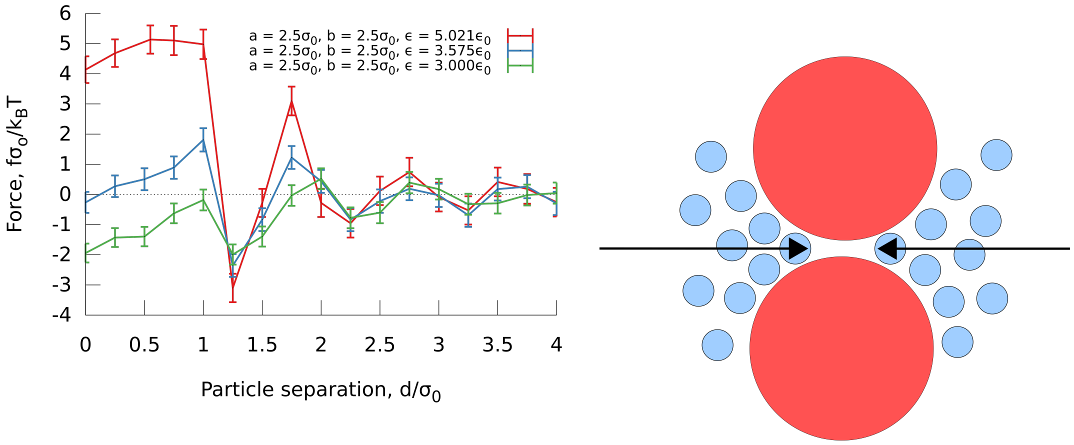

(a) **(b)**

Figure 4.18: **(a)** Solvent-mediated force acting on a spherical nanoparticle of radii $a = b = c = 2.5\sigma_0$ and well depth ratio $\kappa' = 1$ as a function of surface-to-surface separation d. The nanoparticles are submerged in bulk liquid. **(b)** Two spherical nanoparticles (red) with a separation $d < 1\sigma_0$. Fluid particles (blue) are acting on the nanoparticles. If the spherical nanoparticles have a large well depth ϵ_{fp}, the fluid particles will want to stay between the two nanoparticles.

fluid particle around the nanoparticles. At $d = n\sigma_0$, where n is a whole number, there is available room for exactly n fluid particles, which gives a local maximum. However, at larger n, the local maxima are shifted to lower values of d due to the packing of the fluid particles. The force in the region $d > 1\sigma_0$ is greatest for the nanoparticle submerged in the bulk liquid, less for the nanoparticle adsorbed at the liquid-vapour interface and least for the nanoparticle submerged in the bulk vapour. This is because the amount of fluid particles available to act on the two nanoparticles is highest for the bulk liquid and least for the bulk vapour. The depletion region was observed for $d < 1\sigma_0$. Bresme *et al.* [12] conducted similar molecular dynamics simulations of spherical particles of radii $R = 3.5\sigma_0$, with temperature $T^* = 0.8$, bulk densities $\rho_l^* = 0.732$ and $\rho_v^* = 0.019$, and contact angle $\theta = 95 \pm 5°$. They found the force in the depletion region for the nanoparticle adsorbed at the interface to be approximately four times greater than the force in the vapour phase. In the calculations presented in this work however, the force acting on the nanoparticle pair in the vapour phase is much lower than the force acting on the nanoparticles adsorbed at the interface. The magnitude of the force calculated in the work by Bresme *et al.* is very similar to the force calculated in this work. The discrepancies is due to the differences in contact angle θ, phase densities ρ_l and ρ_v, and nanoparticle size.

Figure 4.18a shows the force acting on three nanoparticle-nanoparticle pairs submerged in bulk liquid with well depths $\epsilon_{fp} = 5.021\epsilon_0$, $\epsilon_{fp} = 3.575\epsilon_0$, and $\epsilon_{fp} = 3.0\epsilon_0$. The depletion region $d < 1\sigma_0$ is very different for each case. The nanoparticle pairs with well depth $\epsilon_{fp} = 5.021\epsilon_0$ and well depth $\epsilon_{fp} = 3.575\epsilon_0$ have repulsive depletion regions. However, for the latter case, the depletion force is smaller and it decreases as the separation d decreases. The nanoparticle pair with well depth $\epsilon_{fp} = 3.0\epsilon_0$ has an attractive depletion region. The force as a function of separation signify the stable separation of nanoparticles moving freely in solution. The nanoparticles with a large well depth prefer to maximise the fluid-nanoparticle surface area, while the nanoparticles with a small well depth prefer to minimise the fluid-nanoparticle surface area. In terms of the solid-liquid interface tension γ_{sl}, the nanoparticles with a large well depth have low solid-liquid interface tension, while the nanoparticles with a small well depth have large solid-liquid interface tension. A nanoparticle pair with a large well depth will have fluid particles highly attracted to the nanoparticles. When the nanoparticles are in the depletion region of each other, fluid particles will push in towards the middle of the two nanoparticles, as seen in figure 4.18b. This will push the two nanoparticles away from each other. The fluid particles will also push on the outside of the nanoparticles, pushing the nanoparticles together. The relation between the amount fluid particles pushing in between the nanoparticles and the amount of fluid particles pushing the nanoparticles together determines the behaviour of these nanoparticles in solution. A nanoparticle pair with a small well depth will have fluid particles that are less attracted to the nanoparticles. The fluid particles will prefer to surround other fluid particles, instead of surrounding the nanoparticle. A distribution of nanoparticles with a large well depth, ϵ_{fp}, in bulk liquid will either stay evenly distributed or they may flocculate. They might flocculate with approximately a mean distance $d = 1.6\sigma_0$ which has a small potential energy minimum. However, the energy barrier to become evenly mixed is not large, and a mixture of nanoparticles with a small well depth ϵ_{fp} will aggregate into large clusters. These clusters will either sediment or cream, depending on the particle mass density.

The nanoparticle-nanoparticle van der Waals force was not included in these force calculations, and they need to be considered when predicting the behaviour of the system. These calculations are only of two nanoparticles, and the force will change as the density of nanoparticles increases.

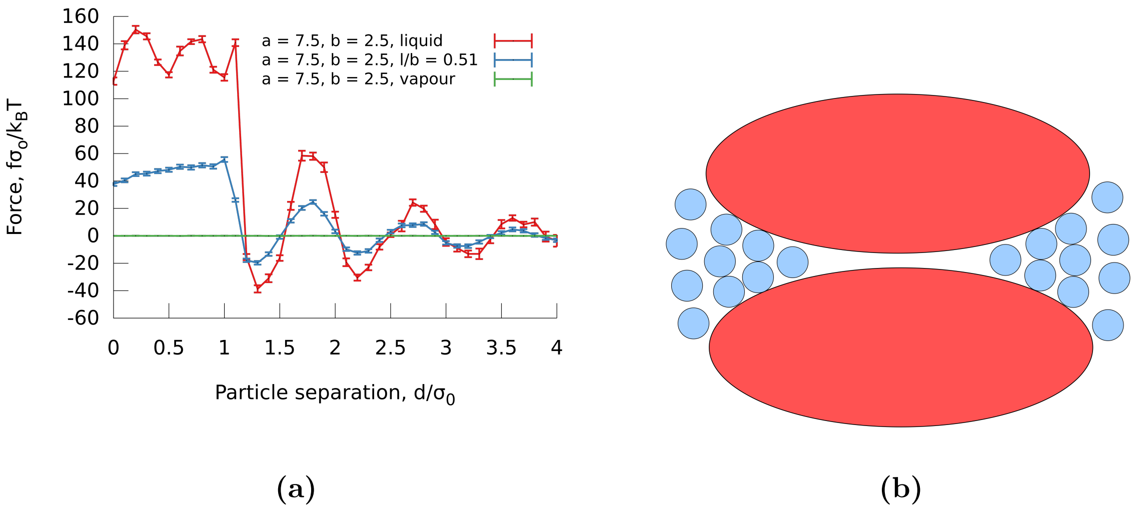

Figure 4.19: **(a)** Solvent-mediated force acting on a prolate ellipsoidal nanoparticle of radii $a = 7.5\sigma_0, b = c = 2.5\sigma_0$ and well depth ratio $\kappa' = 1$ as a function of surface-to-surface separation d in the side-by-side orientation. **(b)** Two prolate ellipsoidal nanoparticles (red) with a separation $d < 1\sigma_0$. Fluid particles (blue) are packing on the tips and creating oscillations in the depletion region.

4.6.2 Prolate ellipsoidal nanoparticles

Prolate ellipsoidal nanoparticles adsorbed at liquid-vapour interfaces are predicted to induce interface deformations, which results in orientation-dependent capillary interactions. The solvent-mediated force acting on prolate ellipsoidal nanoparticles of radii $a = 7.5\sigma_0, b = c = 2.5\sigma_0$ and well depth ratio $\kappa' = 5$ as a function of surface-to-surface separation d is presented in figure 4.19a. This figure shows the force acting on nanoparticles in three different cases: Completely submerged in the liquid phase, completely submerged in the vapour phase, and adsorbed at the liquid-vapour interface with a mean wetting $\langle \frac{l}{b} \rangle = 0.51 \pm 9.52 \times 10^{-5}$. The well depths, ϵ_{fp}, have been set to $\epsilon_{fp} = 25\epsilon_0$, $\epsilon_{fp} = 1\epsilon_0$ and $\epsilon_{fp} = 20\epsilon_0$, respectively. This corresponds to the well depths that give the respective wettabilities. The nanoparticle-nanoparticle pair is in the side-by-side orientation, as seen in figure 2.4a. The force difference between the three different cases are greater for these nanoparticles compared to the spherical particles as presented in figure 4.17b. This is because the well depths ϵ_{fp}, which were equal for all cases in figure 4.17b, varies for each case in this figure. This means that nanoparticles submerged in bulk liquid will form a stronger layer of fluid particles on the nanoparticle surface, while the nanoparticles submerged in the bulk vapour will have a weaker layer of fluid particle on the nanoparticle surface. This explains why the force for the nanoparticle in the li-

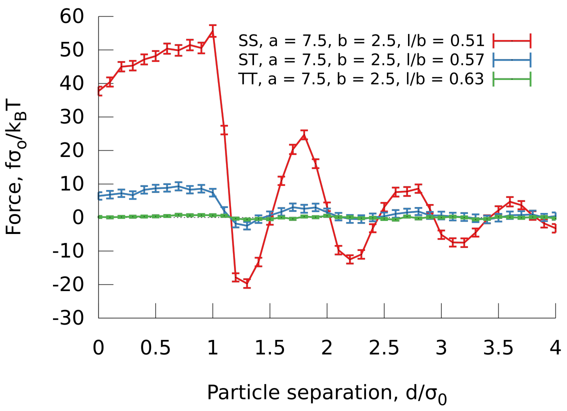

Figure 4.20: Solvent-mediated force acting on a prolate ellipsoidal nanoparticle with well depth ratio $\kappa' = 1$ as a function of surface-to-surface separation d. The nanoparticles are of radii $a = 7.5\sigma_0, b = c = 2.5\sigma_0$ in the side-by-side (SS), side-to-tip (ST) and tip-to-tip (TT) orientations.

quid is much greater in this case, compared to the case presented in figure 4.17b. The magnitude of the force is also much greater for these nanoparticles. This is caused by the size of the nanoparticles, in additions to the well depths. These results suggest that these nanoparticles adsorbed at the liquid-vapour interface will flocculate with approximately a mean distance $d = 1.6\sigma_0$, because the potential energy minimum has a local minimum for that separation. The interaction strength is large for these nanoparticles compared to the spherical particles, suggesting that the flocculation may be stable. However, for a separation $d < 1.6\sigma_0$ they are highly repulsive. The interaction in the vapour phase was minuscule, and it can assume that the nanoparticles will not aggregate or flocculate due to the solvent-mediated forces.

The nanoparticles in the bulk liquid exhibit oscillations of the force in the depletion region $d < 1\sigma_0$. This was not observed for the spherical particle presented in figure 4.17b. This may be explained by packing of fluid particles around the tips of the nanoparticles, as illustrated in figure 4.19b. This type of packing is also present in a spherical particle. However, the curvature of the side of the prolate ellipsoid relative to the size makes this effect much more pronounced. For example, for an oblate ellipsoid with radius $a = b > c$ this effect is expected to be even more pronounced.

Figure 4.20 shows the solvent-mediated force acting on prolate ellipsoidal nanoparticles of radii $a = 7.5\sigma_0, b = c = 2.5\sigma_0$ in three different cases: In the side-by-side orientation, in the side-to-tip orientation, and in the tip-to-tip orientation. The orientations are illustrated in figure 2.4. The force in the side-by-side orientation is greatest, less in the

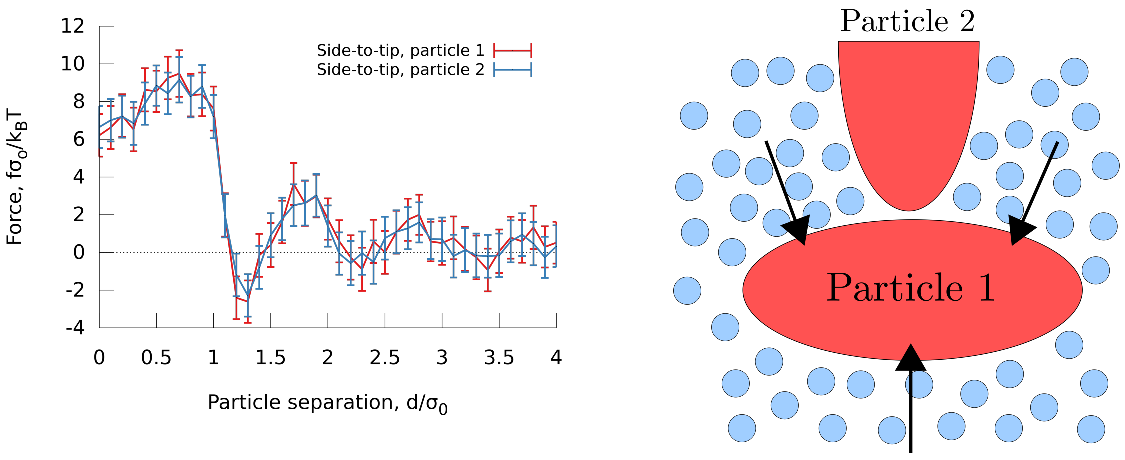

(a) **(b)**

Figure 4.21: **(a)** Nanoparticles of radii $a = 7.5\sigma_0, b = c = 2.5\sigma_0$ in the side-to-tip orientation. This shows that the force on both particles is the same even when the orientation is non-symmetric. **(b)** Two prolate ellipsoidal nanoparticles (red) in the side-to-tip orientation and fluid particles (blue). The fluid particles are pushing on the particle 1 in such a way that the total force on particle 1 equals the total force acting on particle 2.

side-to-tip orientation and least in the tip-to-tip orientation. This may be explained by the area that is available for fluid particles to push or pull the nanoparticles away or towards each other. Two nanoparticles in the side-by-side orientation have a large area that is parallel to the other nanoparticle, while two nanoparticle in the tip-to-tip orientation have a small area. The lateral capillary force, as described by Lehle *et al.* [7] and discussed in section 2.3.3, is expected to be attractive in the side-by-side and tip-to-tip orientations, and repulsive in the side-to-tip orientation. However, this was not observed in these calculations. The lateral capillary force is a direct consequence of interface deformations. In these calculations, the interface deformations are present due to the well depth ratio, implying that the well depth is greater on the side compared to the tip, as presented in section 4.5. This would imply that a lateral capillary force should be present. The potential energy minimum at approximately a mean distance $d < 1.6\sigma_0$ is much greater for the side-by-side orientation compared to the side-to-tip orientation. This implies that the nanoparticles will prefer to aggregate in the side-by-side orientation instead of the side-to-tip orientation. However, this is not caused by the lateral capillary force.

Figure 4.21a shows the force acting on each prolate ellipsoidal nanoparticle in the side-to-tip orientation. The red line shows the force acting on the nanoparticle that has the short radius b pointing towards the other nanoparticle, while the blue line shows

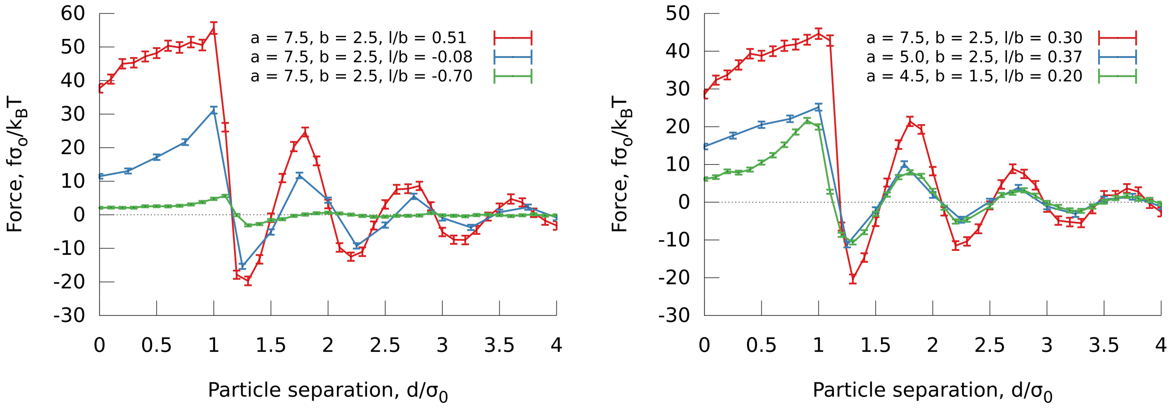

(a) **(b)**

Figure 4.22: Solvent-mediated force acting on a prolate ellipsoidal nanoparticle with well depth ratio $\kappa' = 1$ as a function of surface-to-surface separation d. **(a)** Nanoparticles of radii $a = 7.5\sigma_0, b = c = 2.5\sigma_0$ in the side-by-side orientation, with wettabilities $\frac{l}{b} = 0.51 \pm 9.32 \times 10^{-5}$, $\frac{l}{b} = -0.08 \pm 2.94 \times 10^{-4}$ and $\frac{l}{b} = -0.70 \pm 4.22 \times 10^{-5}$. **(b)** Nanoparticles of radii $a = 7.5\sigma_0, b = c = 2.5\sigma_0$, $a = 5.0\sigma_0, b = c = 2.5\sigma_0$ and $a = 4.5\sigma_0, b = c = 1.5\sigma_0$ in the side-by-side orientation.

the force acting on the nanoparticle that has the long radius a pointing towards the other nanoparticle. One might assume that the nanoparticle with the short radius b pointing towards the other nanoparticle would have a larger force as this nanoparticle has a larger area for the fluid particles to push the nanoparticles together. However, the first nanoparticle also has the highest amount of fluid particles to push the nanoparticle away, illustrated in figure 4.21b. The resulting force is therefore equal for particle 1 and 2.

Figure 4.22a shows the force acting on prolate ellipsoidal nanoparticles of radii $a = 7.5\sigma_0, b = c = 2.5\sigma_0$ and wettabilities $\frac{l}{b} = 0.51 \pm 9.32 \times 10^{-5}$, $\frac{l}{b} = -0.08 \pm 2.94 \times 10^{-4}$ and $\frac{l}{b} = -0.70 \pm 4.22 \times 10^{-5}$. The force acting on the nanoparticle with the highest degree of wetting is greatest, and least for the nanoparticle with the lowest degree of wetting. This is because of the density of fluid particles around the nanoparticle that push and pull the nanoparticle. Figure 4.22b shows the force acting on prolate ellipsoidal nanoparticles of radii $a = 7.5\sigma_0, b = c = 2.5\sigma_0$, $a = 5.0\sigma_0, b = c = 2.5\sigma_0$, and $a = 4.5\sigma_0, b = c = 1.5\sigma_0$. The force acting on the largest nanoparticle is greatest. This is because the amount of area available for the fluid particle to push on the nanoparticles. The nanoparticles of radii $a = 5.0\sigma_0, b = c = 2.5\sigma_0$ and $a = 4.5\sigma_0, b = c = 1.5\sigma_0$ are very similar in the region $d > 1\sigma_0$, but differ in the depletion region $d < 1\sigma_0$. The surface area of the larger nanoparticles is about the two times greater, and they have a higher wettability. The

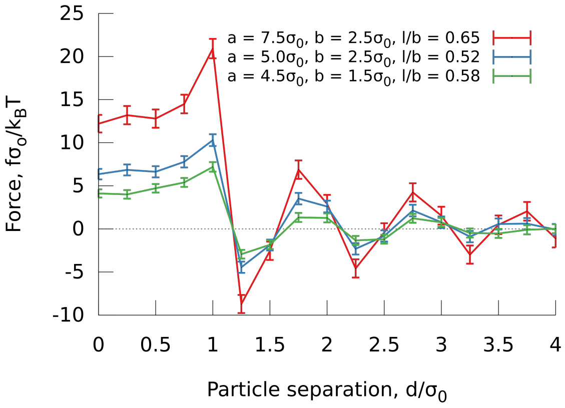

Figure 4.23: Solvent-mediated force acting on a prolate ellipsoidal nanoparticle of radii $a = 7.5\sigma_0, b = c = 2.5\sigma_0$, $a = 5.0\sigma_0, b = c = 2.5\sigma_0$ and $a = 4.5\sigma_0, b = c = 1.5\sigma_0$ with well depth ratio $\kappa' = 1$ as a function of surface-to-surface separation d.

reason why these two nanoparticle sizes are so similar, is likely due to the nanoparticle aspect ratio, κ. The aspect ratio is $\kappa = 2$ for the large nanoparticles, and $\kappa = 3$ for the small nanoparticles. The area of nanoparticles in the side-by-side orientation that pushes the nanoparticles together is greater for nanoparticles with a high aspect ratio κ. For example, the force between two disks and two needles, where the disks and needles have the same surface area, will be greatest for the disks.

Figure 4.23 shows the force acting on nanoparticles of radii $a = 7.5\sigma_0, b = c = 2.5\sigma_0$, $a = 5.0\sigma_0, b = c = 2.5\sigma_0$ and $a = 4.5\sigma_0, b = c = 1.5\sigma_0$ with well depth ratio $\kappa' = 1$ in the side-by-side orientation. This figure shows the same trend as for the nanoparticles with well depth ratio $\kappa' = 1$, but with a weaker force. This is because the nanoparticles with well depth ratio $\kappa' = 5$ create a halo around the sides of the nanoparticle.

4.6.3 Summary of solvent-mediated forces

Nanoparticles will position themselves relative to the liquid-vapour interface in order to have a certain number of fluid particles surrounding them. This means that a highly wetting nanoparticle will be submerged in the bulk liquid, and a partially wetting nanoparticle will adsorb at the liquid-vapour interface. If another nanoparticle is in the depletion range $d < \sigma_0$, it will push away the fluid particles, and the number of fluid particles surrounding the original nanoparticle will decrease. The wetting of the original nanoparticle will no longer be the same, and the fluid particles will push the other nanoparticle away in order to get the same degree of wetting. However, the behaviour is different if the nanoparticle is not at its equilibrium position relative to the liquid-vapour interface. If a nanoparticle with low wettability that is trapped in bulk liquid is considered, as seen in figures 4.17b and 4.18a, it will prefer to have few fluid particles surrounding it. This will result in the fluid particles pushing the nanoparticles together, and the nanoparticles will aggregate in large clusters.

Outside the depletion region $d > \sigma_0$, the nanoparticle pairs are stable at approximately a separation $d = 1.6\sigma_0$. This is because there is room for one fluid particle without causing strain. However, it is unclear how stable this separation is. These results are only of a single nanoparticle pair and with no direct nanoparticle-nanoparticle interaction. More calculations have to be performed to get a better understanding of how a mixture of nanoparticles in a two-phase system will behave.

The prolate ellipsoidal nanoparticles were found to have the same characteristics as the spherical nanoparticles. They have a lower energy minimum at approximately a separation $d = 1.6\sigma_0$ in the side-by-side orientation than in the side-to-tip orientation. This suggests that these nanoparticles will aggregate side-by-side rather than side-to-tip. The lateral capillary interaction was not observed, but it may still be present. This may be investigated by calculating the radial distribution function of several of these nanoparticles adsorbed at a liquid-vapour interface.

Chapter 5

Conclusion

Theory relevant to nanoparticles adsorbed at liquid-vapour interfaces has been presented, a computational method for modelling prolate ellipsoidal nanoparticles interacting with a two-phase system has been presented and several aspects of nanoparticle interaction with liquid-vapour interfaces have been calculated. Several different nanoparticles were considered, including nanoparticles with well depth ratios $\kappa' = 5$ and $\kappa' = 1$, and prolate ellipsoidal and spherical nanoparticle shapes of different sizes.

A molecular dynamics method for modelling prolate ellipsoidal nanoparticles adsorbed at liquid-vapour interfaces has been established. This was done by combining the Gay-Berne force field and the Lennard-Jones force field. The Gay-Berne potential is a problematic force field to use, because the nanoparticle size is not correct when combining large nanoparticles and small fluid particles due to the Perram approximation. A better option might be RE-squared interaction [27].

The wettability was calculated, and the wettability of these nanoparticles was determined. It was found that the equilibrium pitch of highly wetting prolate ellipsoidal nanoparticles with well depth ratio $\kappa' = 5$ is close to $\phi = 0, \pi$. The expected pitch for prolate ellipsoidal nanoparticles is $\phi = \frac{\pi}{2}$, and it was shown that this is the equilibrium pitch for all other prolate ellipsoidal nanoparticles.

The Brownian motion of a prolate ellipsoidal nanoparticle of radii $a = 7.5\sigma_0, b = c = 2.5\sigma_0$ of different wettabilities was compared to a spherical nanoparticle of radius $R = 2.5\sigma_0$. The self-diffusion coefficients were calculated, and it was found that the self-diffusion coefficients were approximately the same for both nanoparticle sizes with the same wettability. The movement of highly wetting prolate ellipsoidal nanoparticles seemed to be primarily parallel to the long axis of the nanoparticle. However, this has to be further investigated for confirmation. The self-diffusion coefficient of the nanoparticles was found to increase exponentially as the wetting of the nanoparticles decreased.

Prolate ellipsoidal nanoparticles adsorbed at fluid interfaces are predicted to deform the interface. The interface deformation was calculated, but a clear deformation due to the nanoparticle shape was not found. This could be because the interface deformation is too small for the nanoparticle aspect ratio and size. However, the interface deformation caused by a well depth ratio $\kappa' = 5$ showed that an interface deformation is possible to observe using the method described.

The forces between nanoparticles adsorbed at liquid-vapour interfaces and submerged in bulk phases were calculated. The force between two spherical nanoparticles was similar to the results by Bresme *et al.* [12]. The force calculated was used in order to predict the behaviour of nanoparticles of this type in a two-phase system. The force between prolate ellipsoidal nanoparticles was calculated for several nanoparticles sizes. Lateral capillary force was not observed. However, the force between prolate ellipsoidal nanoparticles was found to be greater side-by-side compared to side-to-tip and tip-to-tip.

The interface deformation might be possible to observe if the nanoparticle aspect ratio and the nanoparticle size are increased. This might also give an observable lateral capillary interaction. The force calculations should also be compared to force calculations where more than two nanoparticles are present. This might be done by for example calculating the radial distribution function, as done by Bresme *et al.* for spherical nanoparticles [12]. An effective force field might be constructed, such that one would only describe the nanoparticles explicitly and not the fluid particles implicitly. This would reduce the computational cost, while still keeping it realistic.

Appendix A

Force fields

The Gay-Berne force field as described by Evaraers and Ejtehadi [27], discussed in section 3.1.2, does not give the correct nanoparticle size if the nanoparticle is much larger than the fluid particle. This is due to the Perram approximation [29]. This is possible to circumvent if there is no nanoparticle-nanoparticle interaction. Table A.1 presents all Gay-Berne parameters used in the fluid-nanoparticle interaction in this thesis. Figures A.1, A.2 and A.3 present the potential energy of a nanoparticle and a fluid particle as a function of the separation $\|\boldsymbol{r}_{ij}\|$, as the fluid particle approaches the side and the tip of the nanoparticle.

Table A.1: Gay-Berne parameters for fluid-nanoparticle interaction.

κ'	a	$b = c$	$\sigma_{p,x}$	$\sigma_{p,y} = \sigma_{p,y}$	e_{ap}	$e_{bp} = e_{cp}$	r_{fp}	Figure
5	7.5	2.5	$\sqrt{127}$	$\sqrt{17}$	0.2	1	14.0	A.1a
	5.0	2.5	$\sqrt{\frac{119}{2}}$	$\sqrt{17}$	0.2	1	11.5	A.1b
	4.5	1.5	7	$\sqrt{7}$	0.2	1	10.5	A.1c
	1.5	0.5	$\sqrt{7}$	1	0.2	1	6.0	A.1d
1	7.5	2.5	$\sqrt{127}$	$\sqrt{17}$	1	1	14.0	A.2a
	5.0	2.5	$\sqrt{\frac{119}{2}}$	$\sqrt{17}$	1	1	11.5	A.2b
	2.5	2.5	$\sqrt{17}$	$\sqrt{17}$	1	1	8.0	A.3
	4.5	1.5	7	$\sqrt{7}$	1	1	10.5	A.2c
	1.5	0.5	$\sqrt{7}$	1	1	1	6.0	A.2d

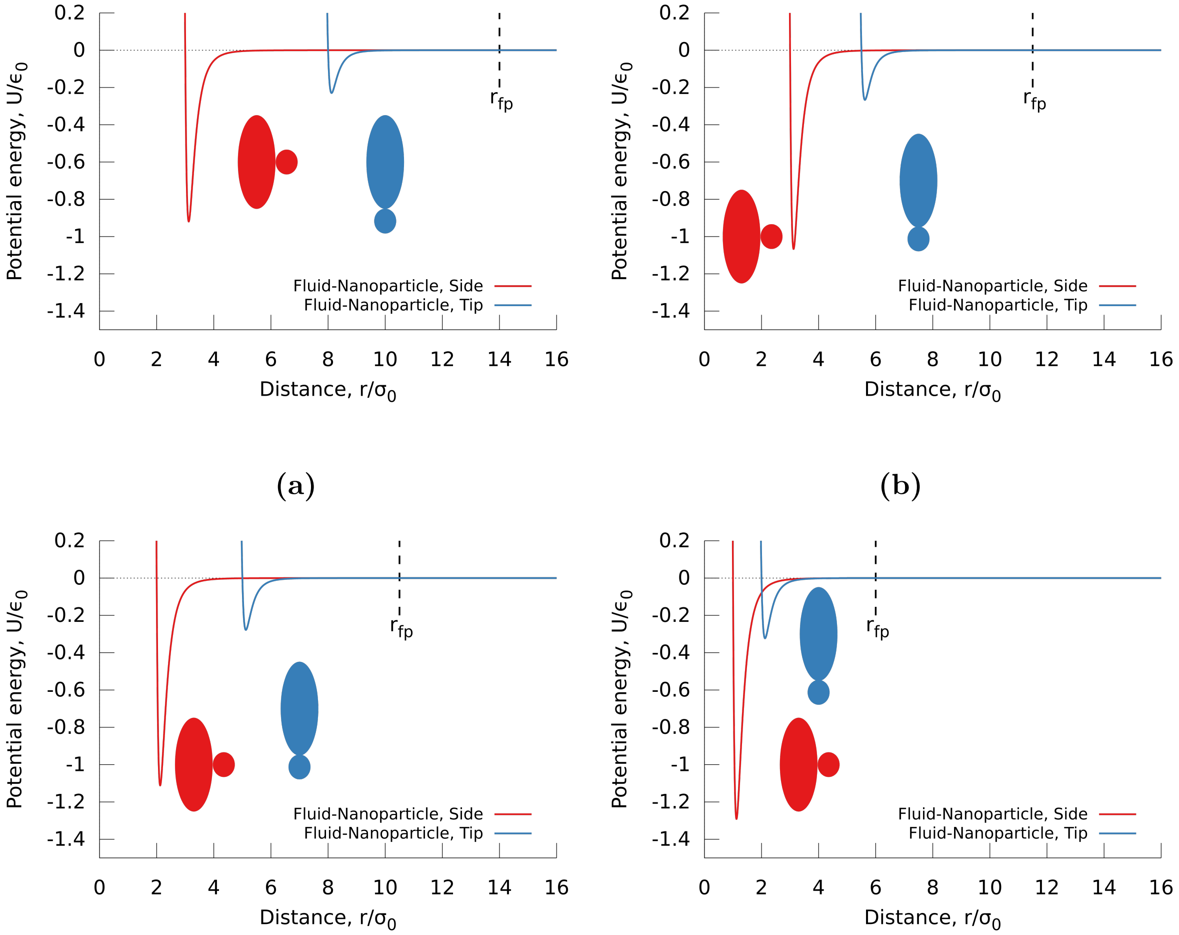

(a)

(b)

(c)

(d)

Figure A.1: Potential energy of the nanoparticle-fluid interaction with well depth ratio $\kappa' = 5$. r_{fp} is the cut-off. **(a)** Nanoparticle of size $a = 7.5\sigma_0, b = c = 2.5\sigma_0$ and well depth $\epsilon_{fp} = 3.0\epsilon_0$, **(b)** nanoparticle of size $a = 5.0\sigma_0, b = c = 2.5\sigma_0$ and well depth $\epsilon_{fp} = 3.0\epsilon_0$, **(c)** nanoparticle of size $a = 4.5\sigma_0, b = c = 2.5\sigma_0$ and well depth $\epsilon_{fp} = 2.0\epsilon_0$ and **(d)** nanoparticle of size $a = 1.5\sigma_0, b = c = 0.5\sigma_0$ and well depth $\epsilon_{fp} = 1.0\epsilon_0$.

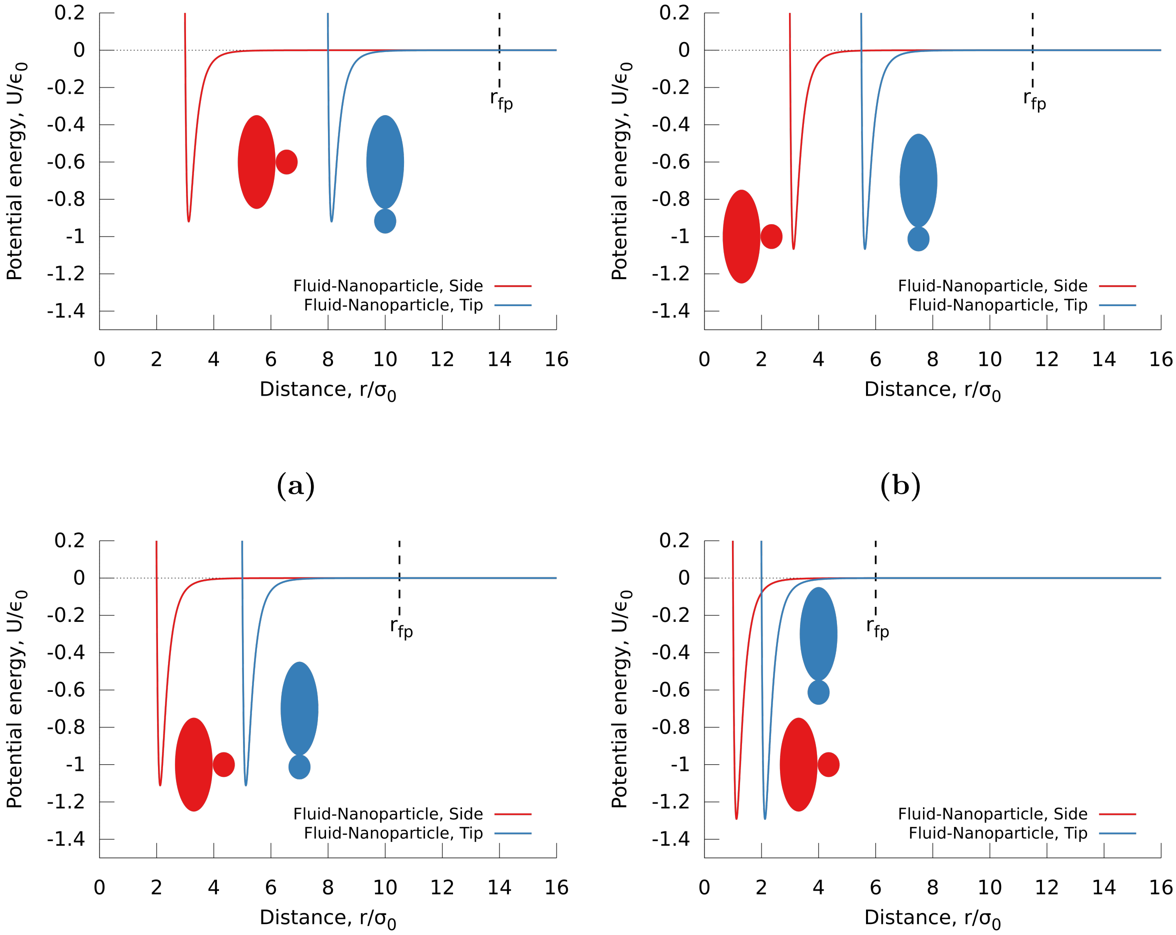

(a) (b)

(c) (d)

Figure A.2: Potential energy of the nanoparticle-fluid interaction with well depth ratio $\kappa' = 1$. r_{fp} is the cut-off. **(a)** Nanoparticle of size $a = 7.5\sigma_0, b = c = 2.5\sigma_0$ and well depth $\epsilon_{fp} = 3.0\epsilon_0$, **(b)** nanoparticle of size $a = 5.0\sigma_0, b = c = 2.5\sigma_0$ and well depth $\epsilon_{fp} = 3.0\epsilon_0$, **(c)** nanoparticle of size $a = 4.5\sigma_0, b = c = 2.5\sigma_0$ and well depth $\epsilon_{fp} = 2.0\epsilon_0$ and **(d)** nanoparticle of size $a = 1.5\sigma_0, b = c = 0.5\sigma_0$ and well depth $\epsilon_{fp} = 1.0\epsilon_0$.

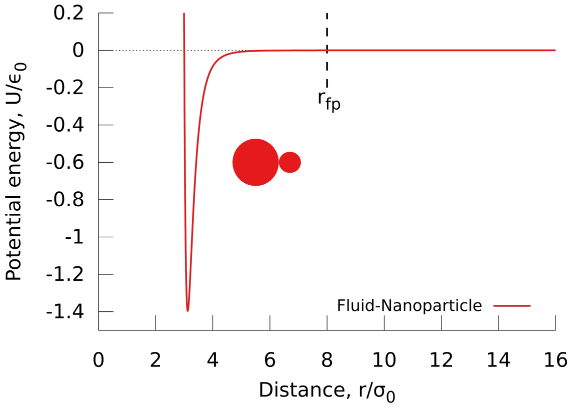

Figure A.3: Potential energy of the nanoparticle-fluid interaction with well depth ratio $\kappa' = 1$ and nanoparticle radii $a = b = c = 2.5\sigma_0$ and well depth $\epsilon_{fp} = 3.0$.

Appendix B

LAMMPS input scripts

The calculations presented in this thesis have been carried out with the molecular dynamics program LAMMPS (Large-scale Atomic/Molecular Massively Parallel Simulator) [1], developed by Sandia National Laboratories [31]. Templates scripts of the different calculations done in this thesis are presented below.

The restart file made by the first script titled "Equilibration" is used as input for the rest of the calculations, with variations in simulation box size.

```
# Comparison with Lennard-Jones crystal
units            lj
atom_style       atomic
atom_modify      map array

region           box block 0 60 0 60 0 60
create_box       2 box
create_atoms     1 single 0 0 30

variable px      equal 15
variable py      equal 15
variable pz      equal 30
variable a       equal 7.5
variable b       equal 2.5
variable c       equal 2.5
```

---

[1] http://lammps.sandia.gov/

```
variable R       equal 0.1
variable d       equal 2^(1.0/6.0)/(2.0*sqrt(2.0))
variable n       equal 20

variable i loop -$n $n
label loop_i
    variable x equal $i*$d+${px}
    variable j loop -$n $n
        label loop_j
            variable y equal $j*$d+${py}
            variable k loop -$n $n
            label loop_k
                variable z equal $k*$d+${pz}
                variable tmp1 equal (($x-${px})/$a)^2 &
                    +(($y-${py})/$b)^2+(($z-${pz})/$c)^2
                variable tmp2 equal ($i+$j+$k)%2
                if "${tmp1} <= 1 && ${tmp2} == 0" then &
                    "create_atoms 2 single $x $y $z"
            next k
            jump SELF loop_k
    next j
    jump SELF loop_j
next i
jump SELF loop_i

mass 1 1
mass 2 1

pair_style       lj/cut 3
pair_coeff       1 1 1 1      3
pair_coeff       1 2 1 0.5    3
pair_coeff       2 2 1 1      3
```

```

neighbor          0.8 bin
neigh_modify      exclude type 2 2

variable          x equal x[1]
variable          y equal y[1]

thermo_style      custom step v_x v_y epair etotal
thermo            3000
thermo_modify     norm no

dump              1 all custom 500 dump.out id type x y z

group             move type 1
group             particle type 2
timestep          0.01
log               force.log

compute           pe move pe/atom pair
dump              2 move custom 1 force.out id type c_pe x y

fix               3 particle rigid single force * off off off torque * off of

variable l loop 0 1500
label loop_l
    variable x equal v_l/50
    set group move x ${x} y 0
    fix move move move linear 0 2 0
    run 1500
next l
jump SELF loop_l
```

```
# Equilibration
restart          5000 melted.*

units            lj
atom_style       ellipsoid

lattice          fcc          0.8
region           box          block 0.0 30 0.0 15 0.0 15
region           liquid       block 7.5 12.5 0.0 15 0.0 15

create_box       2 liquid
create_atoms     1 region liquid

group            solvent type 1
group            solute type 2

set              type 1 mass 1
set              type 2 mass 1
set              type 1 shape 1 1 1
set              type 2 shape 1 1 1

pair_style       gayberne 1 1 1 3
pair_coeff       1 1     1 1     3 3 3    0 0 0    3
pair_coeff       1 2     1 1     0 0 0    0 0 0    0
pair_coeff       2 2     1 1     1 1 1    0 0 0    0

# Calculating orientation
compute          orient all property/atom quati quatj quatk quatw
compute          shape all property/atom shapex shapey shapez
compute          rot all temp/asphere
variable         dof equal 3*count(solvent)+count(solute)+3
compute_modify   rot extra ${dof}
```

```

fix              ensemble all nve/asphere

thermo_style     custom step time c_rot pe ke etotal
thermo           500

dump             dump all custom 500 dump_equil.out id type &
                 x y z c_orient[1] c_orient[2] c_orient[3] &
                 c_orient[4] c_shape[1] c_shape[2] c_shape[3] &

velocity         all create 2.0 87287 loop geom

timestep         0.002
run              5000

restart          15000 equilibration.*
change_box       all     x final 0.0 30
velocity         all scale 0.7

fix              centering1 solvent recenter 15 NULL NULL

run              10000
```

```
# Wetting
read_restart      equilibration.*
restart           50000 restart.%.* nfile 5

lattice           fcc 0.8

region            delete  cylinder y 7.5 7.5 2.5 0 15

delete_atoms      region delete
create_atoms      2 single 7.5 7.5 7.5

set               type 1 mass 1
set               type 2 mass 1
set               type 1 shape 1 1 1
set               type 2 shape sqrt(127) sqrt(17) sqrt(17)

group             solvent type 1
group             solute type 2

set               group solute quat  0 0 1  90

pair_style        gayberne 1 1 1 3
pair_coeff        1 1     1 1     3 3 3   0 0 0 3
pair_coeff        1 2     1 1     0 0 0   0 0 0 14
pair_coeff        2 2     0 1   0.2 1 1   0 0 0 0

compute           cc1 solvent chunk/atom bin/1d x lower 0.5
fix               dens1d solvent ave/chunk 0.1 0.1 0.1 &
                  cc1 density/mass density/number &
                  file density_profile.dat

compute           orient all property/atom quati quatj quatk quatw
compute           shape all property/atom shapex shapey shapez

fix               ensemble all nvt/asphere temp 0.7 0.7 0.2
variable          dof equal 3*count(solvent)
compute_modify    ensemble_temp extra ${dof}

thermo_style      custom step time c_ensemble_temp pe ke etotal
thermo            500

dump              init_dump all custom 500 dump_init.out id type &
                  x y z c_orient[1] c_orient[2] c_orient[3] &
                  c_orient[4] c_shape[1] c_shape[2] c_shape[3]

neighbor          1.50 multi
comm_modify       mode multi cutoff/multi 1 0.50 &
                  cutoff/multi 2 1.50
neigh_modify      delay 0 every 1 check yes &
                  page 5000000 one 500000

fix               centering1 solvent recenter 15 NULL NULL
timestep          0.002
run               10000

dump              dump all custom 500 dump.out id type &
                  x y z c_orient[1] c_orient[2] c_orient[3] &
                  c_orient[4] c_shape[1] c_shape[2] c_shape[3]

run               500000
```

```
# Interface deformation
read_restart      equilibration.*
restart           50000 restart.%.* nfile 5

lattice           fcc 0.8

region            delete  cylinder y 7.5 7.5 2.5 0 15

delete_atoms      region delete
create_atoms      2 single 7.5 7.5 7.5

set               type 1 mass 1
set               type 2 mass 1
set               type 1 shape 1 1 1
set               type 2 shape sqrt(127) sqrt(17) sqrt(17)

group             solvent type 1
group             solute type 2

set               group solute quat  0 0 1  90

pair_style        gayberne 1 1 1 3
pair_coeff        1 1     1 1     3 3 3   0 0 0 3
pair_coeff        1 2     1 1     0 0 0   0 0 0 14
pair_coeff        2 2     0 1   0.2 1 1   0 0 0 0

compute           cc1 solvent chunk/atom bin/1d x lower 0.5
fix               dens1d solvent ave/chunk 0.1 0.1 0.1 &
                  cc1 density/mass density/number &
                  file density_profile.dat

compute           orient all property/atom quati quatj quatk quatw
compute         shape all property/atom shapex shapey shapez

fix             ensemble all nvt/asphere temp 0.7 0.7 0.2
variable        dof equal 3*count(solvent)
compute_modify  ensemble_temp extra ${dof}

thermo_style    custom step time c_ensemble_temp pe ke etotal
thermo          500

dump            init_dump all custom 500 dump_init.out id type &
                x y z c_orient[1] c_orient[2] c_orient[3] &
                c_orient[4] c_shape[1] c_shape[2] c_shape[3]

neighbor        1.50 multi
comm_modify     mode multi cutoff/multi 1 0.50 &
                cutoff/multi 2 1.50
neigh_modify    delay 0 every 1 check yes &
                page 5000000 one 500000

fix             centering1 solvent recenter 15 NULL NULL
timestep        0.002
run             10000

fix             linear_mom solute momentum 1 linear 1 1 1

dump            dump all custom 500 dump.out id type &
                x y z c_orient[1] c_orient[2] c_orient[3] &
                c_orient[4] c_shape[1] c_shape[2] c_shape[3]

run             500000
```

```
# Solvent-mediated force
read_restart     equilibration.*
restart          50000 restart.%.* nfile 5

lattice          fcc 0.8

region           delete1     cylinder y 7.5 5.0 2.5 0 15
region           delete2     cylinder y 7.5 10.0 2.5 0 15
delete_atoms     region delete1
delete_atoms     region delete2
create_atoms     2 single 7.5 7.5 5.0
create_atoms     2 single 7.5 7.5 10.0

set              type 1 mass 1
set              type 2 mass 1
set              type 1 shape 1 1 1
set              type 2 shape sqrt(127) sqrt(17) sqrt(17)

group            solvent type 1
group            solute type 2

set              group solute quat  0 0 1  90

pair_style       gayberne 1 1 1 3
pair_coeff       1 1     1 1      3 3 3   0 0 0 3
pair_coeff       1 2     1 1      0 0 0   0 0 0 14
pair_coeff       2 2     0 1    0.2 1 1   0 0 0 0

compute          cc1 solvent chunk/atom bin/1d x lower 0.5
fix              dens1d solvent ave/chunk 0.1 0.1 0.1 &
                 cc1 density/mass density/number &
                 file density_profile.dat
```

```

compute         orient all property/atom quati quatj quatk quatw
compute         shape all property/atom shapex shapey shapez

fix             ensemble all nvt/asphere temp 0.7 0.7 0.2
variable        dof equal 3*count(solvent)
compute_modify  ensemble_temp extra ${dof}

thermo_style    custom step time c_ensemble_temp pe ke etotal
thermo          500

dump            init_dump all custom 500 dump_init.out id type &
                x y z c_orient[1] c_orient[2] c_orient[3] &
                c_orient[4] c_shape[1] c_shape[2] c_shape[3]

neighbor        1.50 multi
comm_modify     mode multi cutoff/multi 1 0.50 &
                cutoff/multi 2 1.50
neigh_modify    delay 0 every 1 check yes &
                page 5000000 one 500000

fix             centering1 solvent recenter 15 NULL NULL
timestep        0.002
run             10000

dump            dump all custom 500 dump.out id type &
                x y z c_orient[1] c_orient[2] c_orient[3] &
                c_orient[4] c_shape[1] c_shape[2] c_shape[3]

dump            force solute custom 100 force.out id &
                type x y z fx fy fz
run             500000
```

Bibliography

[1] B. J. Ennis, J. Green, and R. Davies. The legacy of neglect in the US. *Chem. Eng. Prog.*, 90(4):32–43, 1994.

[2] Paul C Hiemenz and Raj Rajagopalan. Principles of colloid and surface chemistry. *J. Colloid Interface Sci.*, 70(2):650, 1997.

[3] Z. Rozynek, A. Mikkelsen, P. Dommersnes, and J. O. Fossum. Electroformation of Janus and patchy capsules. *Nat. Commun.*, 5(May):3945, 2014.

[4] P. Dommersnes, Z. Rozynek, A. Mikkelsen, R. Castberg, K. Kjerstad, K. Hersvik, and J. O. Fossum. Active structuring of colloidal armour on liquid drops. *Nat. Commun.*, 4(May):2066, 2013.

[5] G. B. Davies, T. Krüger, P. V. Coveney, J. Harting, and F. Bresme. Assembling ellipsoidal particles at fluid interfaces using switchable dipolar capillary interactions. *Adv. Mater.*, 26(39):6715–6719, 2014.

[6] J. C. Loudet and B. Pouligny. How do mosquito eggs self-assemble on the water surface? *Eur. Phys. J. E*, 34(8), 2011.

[7] H. Lehle, E. Noruzifar, and M. Oettel. Ellipsoidal particles at fluid interfaces. *Eur. Phys. J. E*, 26(1-2):151–160, 2008.

[8] S. Dasgupta, M. Katava, M. Faraj, T. Auth, and G. Gompper. Capillary Assembly of Microscale Ellipsoidal, Cuboidal, and Spherical Particles at Interfaces. *Langmuir*, 30(40):11873–11882, 2014.

[9] F. Bresme and M. Oettel. Nanoparticles at fluid interfaces. *J. Phys. Condens. Matter*, 19(41):413101, 2007.

[10] R. Aveyard and J. H. Clint. Particle wettability and line tension. *J. Chem. Soc. Faraday Trans.*, 92(1):85, 1996.

[11] Jordi Faraudo and Fernando Bresme. Stability of particles adsorbed at liquid/fluid interfaces: Shape effects induced by line tension. *J. Chem. Phys.*, 118(14):6518–6528, 2003.

[12] F. Bresme, H. Lehle, and M. Oettel. Solvent-mediated interactions between nanoparticles at fluid interfaces. *J. Chem. Phys.*, 130(21), 2009.

[13] F. Bresme and N. Quirke. Computer Simulation Study of the Wetting Behavior and Line Tensions of Nanometer Size Particulates at a Liquid-Vapor Interface. *Phys. Rev. Lett.*, 80(17):3791–3794, 1998.

[14] F. Bresme and N. Quirke. Computer simulation of wetting and drying of spherical particulates at a liquid-vapor interface. *J. Chem. Phys.*, 110(7):3536–3547, 1999.

[15] F. Bresme and N. Quirke. Computer simulation studies of liquid lenses at a liquid–liquid interface. *J. Chem. Phys.*, 112(13):5985–5990, 2000.

[16] Bruce M Law, Sean P Mcbride, Jiang Yong Wang, Haeng Sub Wi, Govind Paneru, Santigo Betelu, Baku Ushijima, Youichi Takata, Bret Flanders, Fernando Bresme, Hiroki Matsubara, Takanori Takiue, and Makoto Aratono. Line tension and its influence on droplets and particles at surfaces. *Prog. Surf. Sci.*, 92(1):1–39, 2017.

[17] J. Faraudo and F. Bresme. Stability of particles adsorbed at liquid/fluid interfaces: Shape effects induced by line tension. *J. Chem. Phys.*, 118(14):6518–6528, 2003.

[18] R K Pathria and Paul D. Beale. *Statistical Mechanics.* 2011.

[19] Peter A. Kralchevsky and Kuniaki Nagayama. Capillary interactions between particles bound to interfaces, liquid films and biomembranes. *Adv. Colloid Interface Sci.*, 85(2):145–192, 2000.

[20] G. B. Davies, T. Krüger, P. V. Coveney, J. Harting, and F. Bresme. Interface deformations affect the orientation transition of magnetic ellipsoidal particles adsorbed at fluid-fluid interfaces. *Soft Matter*, 10(35):6742–8, 2014.

[21] David F. Williams and John C. Berg. The aggregation of colloidal particles at the air-water interface. *J. Colloid Interface Sci.*, 152(1):218–229, 1992.

[22] L. Verlet. Computer "Experiments" on Classical Fluids. I. Thermodynamical Properties of Lennard-Jones Molecules. *Phys. Rev.*, 159(1), 1967.

[23] D. J. Evans and S. Murad. Singularity free algorithm for molecular dynamics simulation of rigid polyatomics. *Mol. Phys.*, 34(2):327–331, 1977.

[24] M.P. Allen and G. Germano. Expressions for forces and torques in molecular simulations using rigid bodies. *Mol. Phys.*, 104(20-21):3225–3235, 2006.

[25] M. P. Allen and D. J. Tildesley. Computer Simulation of Liquids. *Oxford Univ. Press. New York*, 1987.

[26] J. G. Gay and B. J. Berne. Modification of the overlap potential to mimic a linear site–site potential. *J. Chem. Phys.*, 74(6):3316, 1981.

[27] R. Everaers and M. R. Ejtehadi. Interaction potentials for soft and hard ellipsoids. *Phys. Rev. E. Stat. Nonlin. Soft Matter Phys.*, 67(4 Pt 1):041710, 2003.

[28] W. M. Brown, M. K. Petersen, S. J. Plimpton, and G. S. Grest. Liquid crystal nanodroplets in solution. *J. Chem. Phys.*, 130(4), 2009.

[29] John. W. Perram, John Rasmussen, Eigil Præstgaard, and Joel L. Lebowitz. Ellipsoid contact potential: Theory and relation to overlap potentials. *Phys. Rev. E*, 54(6):6565–6572, 1996.

[30] William G. Hoover. Canonical dynamics: Equilibrium phase-space distributions. *Phys. Rev. A*, 31(3):1695–1697, 1985.

[31] S. Plimpton. Fast Parallel Algorithms for Short – Range Molecular Dynamics. *J. Comput. Phys.*, 117(June 1994):1–19, 1995.

[32] M. Babadi, R. Everaers, and M. R. Ejtehadi. Coarse-grained interaction potentials for anisotropic molecules. *J. Chem. Phys.*, 124(17), 2006.

[33] Roberto Berardi, Alberto Costantini, Luca Muccioli, Silvia Orlandi, and Claudio Zannoni. A computer simulation study of the formation of liquid crystal nanodroplets from a homogeneous solution. *J. Chem. Phys.*, 126(4), 2007.

[34] Julian Brown, Michael Allen, Elvira Martín del Río, and Enrique Miguel. Effects of elongation on the phase behavior of the Gay-Berne fluid. *Phys. Rev. E*, 57(6):6685–6699, 1998.

[35] M Cheshire, W Massey, and M Jauch. Phase Transitions of the Lennard-Jones System. 0579, 1964.

[36] B. Smit. Phase diagrams of Lennard-Jones fluids. *J. Chem. Phys.*, 96(11):8639–8640, 1992.

[37] B. Widom J. S. Rowlinson. *Molecular theory of capillarity*, volume 167. 1982.

[38] John G Kirkwood and Frank P Buff. The Statistical Mechanical Theory of Surface Tension. *J. Chem. Phys.*, 17(3):338–343, 1949.